Journal for ImmunoTherapy of Cancer

Hypoxia-induced RCOR2 promotes macrophage M2 polarization and CD8$^+$ T-cell exhaustion by enhancing LIF transcription in hepatocellular carcinoma

Wenbo Jia,[1,2] Jinyi Wang,[1,2] Weiming Yang,[3] Zhijie Ding,[3] Litao Liang,[1,2] Chao Xu,[1,2] Yanzhi Feng,[1,2] Qingpeng Lv,[1,2] Deming Zhu,[1,2] Wenhu Zhao,[1,2] Xiangyu Ling,[1,2] Yong Yan,[3] Xiaoming Ai,[4] Yongping Zhou,[3] Lianbao Kong,[1,2] Wenzhou Ding [1,2]

To cite: Jia W, Wang J, Yang W, *et al*. Hypoxia-induced RCOR2 promotes macrophage M2 polarization and CD8$^+$ T-cell exhaustion by enhancing LIF transcription in hepatocellular carcinoma. *Journal for ImmunoTherapy of Cancer* 2025;**13**:e012314. doi:10.1136/jitc-2025-012314

► Additional supplemental material is published online only. To view, please visit the journal online (https://doi.org/10.1136/jitc-2025-012314).

WJ and JW contributed equally.

WJ and JW are joint first authors.

Accepted 15 September 2025

For numbered affiliations see end of article.

Correspondence to
Dr Wenzhou Ding;
dingwenzhou@njmu.edu.cn

Mr Lianbao Kong;
lbkong@njmu.edu.cn

Mr Yongping Zhou;
zyp19840527@aliyun.com

Mr Xiaoming Ai;
aixiaoming0503@163.com

ABSTRACT

Background The hypoxic microenvironment plays a crucial role in regulating the progression of hepatocellular carcinoma (HCC) and facilitating immune evasion. It is essential to gain a more comprehensive understanding of the pathways through which hypoxia influences HCC progression and immune evasion.

Methods We employed RNA sequencing, The Cancer Genome Atlas (TCGA) data analysis, clinical data analysis of HCC, and tissue microarray immunohistochemical analysis to identify key genes associated with hypoxia regulation and immune evasion. We investigated the biological functions of REST corepressor 2 (RCOR2) in tumor progression and immune evasion through mass cytometry, multiplex immunofluorescence, an orthotopic liver transplantation tumor model, in vitro co-culture systems, flow cytometry, and immunohistochemical analysis. Additionally, we used molecular techniques such as RNA sequencing, chromatin immunoprecipitation sequencing, and mass spectrometry to gain deeper insights into the potential molecular mechanisms underlying RCOR2.

Results We found that the hypoxia-related factor RCOR2 is upregulated in HCC and is associated with a poor prognosis. RCOR2 enhances the glycolytic process in HCC cells, thereby promoting the proliferation and metastasis of HCC cells under hypoxic conditions. Additionally, RCOR2 facilitates the M2 polarization of macrophages and contributes to the exhaustion of CD8$^+$ T cells. Mechanistically, the hypoxic microenvironment increases the expression of RCOR2 through hypoxia-inducible factor 1-alpha. Concurrently, this microenvironment inhibits the ubiquitin-mediated degradation of RCOR2 by promoting its sumoylation, which facilitates its translocation to the nucleus. The sumoylation of RCOR2 further enhances the transcriptional activity of leukemia inhibitory factor (LIF). LIF, derived from HCC, contributes to the M2 polarization of macrophages, thereby facilitating immune evasion and playing a role in resistance to programmed cell death protein 1 (PD-1) therapies.

Conclusions Our research reveals that the RCOR2/LIF axis within the hypoxic microenvironment of HCC plays a significant role in immune evasion and identifies novel biomarkers associated with tumor resistance to anti-PD-1 therapy. This study provides potential therapeutic targets for HCC.

WHAT IS ALREADY KNOWN ON THIS TOPIC

⇒ The hypoxic microenvironment is a critical factor influencing the response to immunotherapy.

⇒ REST corepressor 2 (RCOR2) is a co-repressor of REST, functioning as an inflammatory regulatory factor and participating in the regulation of antitumor immunity.

WHAT THIS STUDY ADDS

⇒ RCOR2 enhances glycolysis in hepatocellular carcinoma (HCC) cells, thereby promoting their proliferation and metastasis.

⇒ RCOR2 facilitates the M2 polarization of macrophages and contributes to CD8$^+$ T-cell exhaustion by enhancing leukemia inhibitory factor (LIF) transcription.

⇒ The hypoxic microenvironment inhibits the ubiquitin-mediated degradation of RCOR2 by promoting its sumoylation.

⇒ The RCOR2/LIF axis is implicated in resistance to programmed cell death protein-1.

HOW THIS STUDY MIGHT AFFECT RESEARCH, PRACTICE OR POLICY

⇒ Our research indicates that the hypoxia-related factor RCOR2 is associated with a poor prognosis in HCC. The RCOR2/LIF axis plays a crucial role in regulating immune evasion in HCC, and our study identifies new potential targets for HCC immunotherapy.

INTRODUCTION

Hepatocellular carcinoma (HCC) is one of the most prevalent malignant tumors in humans.[1 2] Due to the asymptomatic nature of early-stage HCC, most patients are diagnosed

at an advanced stage. Therefore, identifying novel molecular markers for the onset and progression of HCC is essential for the development of innovative treatments and clinical diagnostics.

The tumor microenvironment is characterized by a dynamic gradient of oxygen diffusion and consumption, where competition among proliferating tumor cells restricts the availability of oxygen and nutrients, resulting in hypoxia in approximately 50% of solid tumors.[3] The capacity of tumors to adapt to discrepancies in oxygen supply and demand leads to increased genomic instability.[4 5] This adaptive response is associated with immune suppression, the protective evolution of tumor stem cells, and a heightened tendency for distant metastasis.[6 7] Hypoxia plays a critical regulatory role in various aspects of HCC, including cell proliferation, metastasis, metabolic pathways, and angiogenesis. Therefore, exploring the regulatory mechanisms by which hypoxia affects HCC cells is of utmost importance.

Recently, immune checkpoint blockade therapy has shown promising results in the treatment of HCC; however, the benefits for most patients remain limited. The hypoxic microenvironment is a critical factor influencing the response to immunotherapy.[8] Metabolic reprogramming and lactic acid accumulation resulting from hypoxia contribute to immune evasion. Within the tumor hypoxic microenvironment, the increased uptake and metabolic activation of glucose and glutamine by tumor cells lead to a depletion of essential nutrients in the tumor microenvironment (TME).[9] This nutrient deficiency results in diminished metabolic activity in effector T cells and promotes an exhausted phenotype.[10 11] Immunosuppressive cells, including regulatory T cells (Tregs), M2-like tumor-associated macrophages (TAMs), and myeloid-derived suppressor cells, can use fatty acid oxidation to generate cellular energy, thereby further sustaining immunosuppression against effector T cells under hypoxic conditions.[12 13] Ultimately, these metabolic alterations in both immune effector cells and immunosuppressive cells hinder the effectiveness of antitumor immune responses. By modulating the metabolism of hypoxia-induced tumor cells and immunosuppressive cells, it may be possible to enhance antitumor immune responses and inhibit tumor growth.[14] Therefore, investigating the mechanisms underlying tumor hypoxia and the regulatory effects of the hypoxic microenvironment on immune cells is of significant importance.

REST corepressor 2 (RCOR2) is a co-repressor of REST, primarily expressed in embryonic stem cells (ESCs), and plays a crucial role in regulating ESC pluripotency and neurogenesis.[15] It is involved in various cellular functions, including the induction of cell differentiation, maintenance of self-renewal, and epigenetic modifications across different cell types.[16] Current research suggests that RCOR2 functions as an inflammatory regulatory factor. It can promote the differentiation of leukemia-initiating cells by trans-activating RUNX1, thereby facilitating the onset of leukemia.[17] Furthermore, the absence of RCOR2 contributes to the dysfunction of Foxp3+Tregs, which enhances antitumor immunity.[18] Additionally, RCOR2 is associated with the upregulation of interleukin (IL)-6 expression in astrocytes, thereby inducing age-related inflammation.[19] To date, there have been no reports on the role of RCOR2 in immune regulation within the context of HCC.

This study demonstrates that hypoxia-induced RCOR2 is upregulated in HCC and is negatively correlated with HCC prognosis. RCOR2 promotes the proliferation and metastasis of HCC cells under hypoxic conditions and enhances the glycolytic process in HCC cells. Additionally, RCOR2 facilitates the polarization of TAMs toward the M2 phenotype and induces $CD8^+$ T-cell exhaustion by enhancing the transcription of leukemia inhibitory factor (LIF). Mechanistically, hypoxia promotes the transcription of RCOR2 through hypoxia-inducible factor 1-alpha (HIF1α), inhibits its ubiquitin-proteasome degradation by promoting sumoylation, and facilitates its nuclear translocation. Furthermore, the RCOR2/LIF axis is involved in regulating responses to programmed cell death protein-1 (PD-1) therapy. Our study uncovers a novel mechanism of immune evasion in HCC and identifies new indicators related to tumor resistance to anti-PD-1 therapy. This research provides potential therapeutic targets for HCC.

MATERIALS AND METHODS

Human tissues

HCC tissues, along with adjacent non-cancerous samples, were collected from patients at the Hepatobiliary Center of the First Affiliated Hospital of Nanjing Medical University. The research involving human subjects was conducted in accordance with the ethical standards established by the World Medical Association, as outlined in the Declaration of Helsinki.

Cell culture

Human HCC cells lines Huh7, MHCC97H, HepG2, Hep3B, HCCLM3, SK-Hep1, YY8103, immortalized human hepatocyte THLE-3 cells, mouse HCC cell line Hepa1-6, myeloid cell line THP1 and human embryonic kidney cell line 293T (HEK-293T) cells were obtained from the Shanghai Institute of Cell Biology, Chinese Academy of Sciences (Shanghai, China). All cells were cultured in Dulbecco's Modified Eagle's Medium (DMEM) or Roswell Park Memorial Institute 1640 (RPMI-1640) medium (Invitrogen, Carlsbad, USA) supplemented with 10% fetal bovine serum (Gibco, Carlsbad, USA) and 50 U/mL penicillin-streptomycin (Invitrogen). The cells were cultured in a 5% CO_2 incubator at 37°C. For the purpose of hypoxia treatment, the cells were cultured in a hypoxic incubator with 1% O_2 and 5% CO_2.

Cell transfection

Lipofectamine 3000 (Invitrogen) was used for the transfection of plasmids and siRNA, adhering to the provided protocol. For lentiviral transfection, polybrene

(Invitrogen) was incorporated to enhance transfection efficiency. Puromycin (Invitrogen) was employed to select for stably transfected cells. Transfection efficiency was assessed using western blot analysis. Lentivirus, siRNA, and plasmids were supplied by GenePharma (Shanghai, China). The specific siRNA and shRNA sequences used in this experiment are detailed in online supplemental table 1.

Quantitative real-time PCR

Total RNA was extracted from cells using the RNA extraction kit provided by Invitrogen. Subsequently, the total RNA was converted to complementary DNA through reverse transcription with the PrimeScript RT Kit (TaKaRa, Dalian, China). Real-time quantitative PCR was performed using SYBR Premix Ex Taq II (TaKaRa) in conjunction with the ABI 7900 PCR system (Applied Biosystems, California, USA). The primer sequences employed in this study are detailed in online supplemental table 2.

Western blot assay

Cells were lysed in pre-chilled radioimmunoprecipitation assay (RIPA) buffer, followed by the addition of 1 mM phenylmethylsulfonyl fluoride. Subsequently, a loading buffer was incorporated, and the mixture was heated at 95°C for 10 min to denature the proteins. The proteins were then separated via sodium dodecyl sulfate-polyacrylamide gel electrophoresis and transferred to a polyvinylidene fluoride membrane (Bio-Rad, California, USA). The membrane was incubated with the primary antibody overnight at 4°C, followed by incubation with the secondary antibody at room temperature for 2 hours. Protein visualization was achieved using enhanced chemiluminescence (Yesen, Shanghai, China). A detailed list of the antibodies used is provided in online supplemental table 3.

Tissue microarrays

A total of 40 pairs of HCC tissues and adjacent non-cancerous tissues were obtained from surgical resections performed at the Hepatobiliary Center of the First Affiliated Hospital of Nanjing Medical University. The collected tissues were fixed in formaldehyde and subsequently prepared into HCC tissue microarrays (TMAs) by Servicebio (Wuhan, China).

Cell counting kit-8 analysis

The cells were seeded in a 96-well plate following transfection. Cell counting kit-8 (CCK-8) solution (RiboBio, Guangzhou, China) was added every 24 hours in accordance with the manufacturer's protocol. The absorbance of each group was measured at a wavelength of 450 nm. Continuous measurements were conducted over a period of 5 days.

5-ethynyl-20-deoxyuridine assay

The 5-ethynyl-20-deoxyuridine (EdU) assay was conducted using the Cell-Light EdU Apollo488 In Vitro Kit (RiboBio). Transfected cells were incubated with EdU solution in a 24-well plate for 2 hours. Following incubation, the cells were fixed with formaldehyde and permeabilized using 0.5% Triton X-100. Subsequently, the cells were stained with Apollo solution, while the nuclei were stained with 4',6-diamidino-2-phenylindole (DAPI). Images were captured using a fluorescence microscope.

Transwell assay

In the cell migration experiment, 600 µL of DMEM supplemented with 10% fetal bovine serum (FBS) was added to the lower chamber of the Transwell (Corning, New York, USA). Subsequently, 200 µL of serum-free DMEM containing 2×10^4 cells was added to the upper chamber of the Transwell. After 48 hours of cell culture, the cells in the upper chamber were removed using a cotton swab, while the cells in the lower chamber were fixed and stained for quantitative analysis. For the invasion experiment, Matrigel (BD Biosciences, New Jersey, USA) was applied to the upper chamber of the Transwell in advance and incubated at 37°C for 2 hours. The remaining steps were identical to those of the migration experiment.

RNA sequencing

For hypoxic HCC cell sequencing, three pairs of Huh7 and YY8103 cells were cultured under normoxic and hypoxic conditions for 48 hours, respectively. The cells were then lysed using TRIzol reagent. For the subsequent sequencing of RCOR2, three pairs of Hep3B cells, known for their overexpression of RCOR2, along with their corresponding negative control cells, were also lysed using TRIzol reagent. RNA sequencing (RNA-seq) was subsequently performed by the Beijing Genomics Institute (Guangzhou, China).

Glucose consumption

Glucose consumption in the HCC cell lines was assessed using a glucose uptake colorimetric assay kit (Sigma-Aldrich). Following transfection, the cells were plated in a 96-well plate and incubated overnight in 100 mL of serum-free medium. Subsequently, 100 µL of KRPH buffer containing 2% bovine serum albumin (BSA) was applied for glucose starvation for 40 min. Next, 10 µL of 10 mM 2-deoxyglucose was added, and the mixture was incubated at 37°C for 1 hour. After washing the cells three times with phosphate-buffered saline (PBS), they were lysed with 80 µL of extraction buffer. The lysate was then frozen in liquid nitrogen and subsequently heated at 90°C for 40 min. After cooling on ice for 5 min, 12 µL of neutralization buffer was added to degrade nicotinamide adenine dinucleotide phosphate (NADP). The mixture was centrifuged at 12,000 g for 5 min, and the supernatant was collected. Finally, 38 µL of the reaction mixture was added to each well, and the absorbance was measured at 412 nm using a microplate reader.

Lactate production

According to the manufacturer's operating procedures, use the L-Lactate Assay Kit (Beyotime) to measure lactate production. Seed the transfected cells into a 96-well cell culture plate and incubate at 37°C overnight. After a 2-hour starvation period, collect the supernatant and add the WST-8 Working Solution. Incubate in the dark at 37°C for 30 min. Measure the lactate production level at 450 nm using a microplate reader.

ATP production

To assess ATP production, the ATP assay kit (Beyotime) was used according to the manufacturer's instructions. ATP lysis buffer was used to homogenize the lysate of the transfected liver cancer cells. Centrifuge at 12,000 g for 5 min at 4°C, and then collect the supernatant. A total of 100 µL of the ATP detection working solution and 50 µL of the supernatant were added to each well, and the relative light unit value was measured using a chemiluminescence instrument.

Extracellular acidification rate and oxygen consumption rate

Extracellular acidification rate (ECAR) and oxygen consumption rate (OCR) assays were performed using a Seahorse Bioscience XF24 extracellular flux analyzer (Seahorse Bioscience). Briefly, HCC cells were seeded onto a Seahorse plate (2×10^5 cells/well). For the ECAR measurement, 175 µL of buffer, along with 25 µL of glucose (10 mmol/L), 25 µL of oligomycin (1 mmol/L), and 25 µL of 2-deoxy-glucose (100 mmol/L), were automatically injected. The Seahorse XF-24 software was used to calculate the ECAR values using the following equations: glycolysis rate = (maximum values before oligomycin injection) − (last values before glucose injection) and glycolytic capacity = (maximum values after oligomycin injection) − (last values before glucose injection). For the OCR measurement, 175 µL of buffer, along with 25 µL of oligomycin (1 mmol/L), 25 µL of fluoro-carbonyl cyanide phenylhydrazone (FCCP) (0.1 mmol/L), and 25 µL of rotenone (0.1 mmol/L), were automatically injected. The Seahorse XF-24 software was employed to determine the OCR values using the following equations: basal respiratory rate = (maximum values before oligomycin injection) − (last values before FCCP injection) and maximum respiratory rate = (maximum values before rotenone injection) − (last values before FCCP injection).

$CD8^+$ T-cell isolation and culture

The Ficoll (Sigma-Aldrich) density gradient centrifugation method was employed to separate human peripheral blood mononuclear cells (PBMCs) according to the provided instructions. 50 ng/mL of recombinant human IL-4 (PeproTech, USA) and 100 ng/mL of granulocyte-macrophage colony-stimulating factor (PeproTech, USA) were added to the PBMCs and cultured for 7 days. Subsequently, heat-stimulated HCC cells were added and co-cultured for 1 day to obtain HCC antigen-loaded antigen-presenting cells.

A $CD8^+$ T-cell isolation kit (Miltenyi Biotec, Germany) was used to isolate the initial CD8+T cells. The T cells were cultured in CTS AIM V SFM (Gibco, New York, USA), supplemented with 1 µg/mL CD3 monoclonal antibody (mAb) (Miltenyi Biotec), 5 µg/mL CD28 mAb (Miltenyi Biotec), and 20 ng/mL recombinant human IL-2 (PeproTech, USA). The cell density was adjusted to 1×10^6 cells per milliliter. The culture medium was refreshed every 3 days. Antigen-responsive $CD8^+$ T cells were obtained by co-culturing HCC antigen-loaded antigen-presenting cells with the initial CD8+T cells at a ratio of 10:1 for 3 days.

Co-culture assay

6-well Transwell chambers (0.4 µm pores, Corning) were used for cell co-culture experiments. In the co-culture of CD8+T cells and HCC cells, activated $CD8^+$ T cells and HCC cells were cultured in a 2:1 ratio, with $CD8^+$ T cells placed in the lower chamber and HCC cells in the upper chamber for 24 hours.

For the co-culture of macrophages and HCC cells, add 100 ng/mL of phorbol 12-myristate 13-acetate (PMA) (PeproTech) to THP-1 cells and culture them for 48 hours to promote their differentiation into macrophages. Subsequently, seed 1×10^6 macrophages in the lower chamber and place 5×10^5 HCC cells in the upper chamber for a co-culture period of 48 hours.

In the co-culture experiment involving CD8+T cells and macrophages, macrophages were initially co-cultured with HCC cells following the previously described steps. Subsequently, 1×10^6 co-cultured macrophages were seeded in the upper chamber, while 1×10^6 CD8+ T cells were introduced into the lower chamber for a 24-hour co-culture period. Following the co-culture period, various detection methods, including quantitative real-time PCR (qRT-PCR), flow cytometry, and ELISA, were used to analyze the results.

Flow cytometry analysis

Mouse liver non-parenchymal cells (NPCs) were isolated by dissociating Hepa1-6 subcutaneous tumors in the presence of collagenase IV (0.1% w/v, Sigma) and DNase (0.005% w/v, Sigma) for 1 hour before centrifugation on a discontinuous Percoll gradient (Sigma-Aldrich). The isolated NPCs were then incubated with TruStain FcX (BioLegend) for 10 min on ice. All subsequent primary antibodies were stained for 30 min on ice. Then, all samples were incubated with LIVE/DEAD fixable blue dead cell stain (Thermo Fisher Scientific) to determine viability. Macrophages were identified as Live/CD45+/F4/80+, while M2 macrophages were characterized using CD206+. $CD8^+$ T cells were gated on Live/CD45+/CD3+/CD8+. The functionality of $CD8^+$ T cells was assessed by measuring PD-1, cytotoxic T-lymphocyte antigen -4 (CTLA-4), and granzyme B (GzmB) levels.

For the flow cytometric identification of in vitro cell experiments, $CD8^+$ T cells and macrophages that were co-cultured were incubated with TruStain FcX (BioLegend) for 10 min on ice. All subsequent primary

antibodies were applied for 30 min on ice. Following this, all samples were incubated with LIVE/DEAD Fixable Blue Dead Cell Stain (Thermo Fisher Scientific) to assess cell viability. The flow cytometry assay was conducted using the BD FACSCanto II. All flow cytometry antibodies used in the experiment were obtained from BioLegend, with detailed information provided in the online supplemental table 3.

ELISA

In a 96-well plate, 100 µL of antibody solution (5 µg/mL) was added to each well and allowed to incubate overnight at 4°C. After removing the antibody solution, add the cell supernatant and incubate at 37°C for 2 hours. Next, introduce the detection antibody solution and incubate at 37°C for an additional 2 hours. Following this, add the streptavidin-HRP working solution (Thermo Scientific, Massachusetts, USA) and incubate at room temperature for 1 hour. Then, add the 3,3',5,5'-Tetramethylbenzidine (TMB) substrate solution (Thermo Scientific) and incubate at room temperature for 30 min. The optical density was measured at 450 nm using a microplate reader. A detailed list of the antibodies used can be found in online supplemental table 3.

Chromatin immunoprecipitation assays

The chromatin immunoprecipitation (ChIP) kit (Beyotime) was used for ChIP detection. Briefly, after cell lysis, chromatin is fragmented to a size range of 200–2,000 base pairs using an ultrasonic cell disruptor, and then immunoprecipitated with anti-RCOR2 and IgG antibodies. Primers are designed based on the promoter of the target gene (see online supplemental table 2). The enriched DNA fragments are subsequently analyzed using quantitative PCR.

Luciferase reporter assay

The LIF promoter sequence was obtained from the UCSC database, and the LIF promoter regions (−2,000/100, −1,500/100, −1,000/100, −500/100, and −2,000/−1,500) were cloned into the pGL4-Basic vector (Promega, Wisconsin, USA) to construct a luciferase reporter gene. Both the wild-type (WT) and mutated forms of the LIF and RCOR2 promoters were also inserted into the pGL4-Basic vector. The resulting plasmids were transfected into 293T cells using Lipofectamine 3000 (Invitrogen). Dual-luciferase reporter assays were conducted using the Dual-Luciferase Reporter Assay System (Promega).

Animal models

In this research, ethical approval for all animal experiments was obtained from the Institutional Animal Care and Use Committee (IACUC) at the First Affiliated Hospital of Nanjing Medical University. All procedures involving animals adhered to the operating guidelines established by the IACUC. 4-week-old male BALB/c Nude and C57BL/6 mice were procured from Vital River (Beijing, China).

Subcutaneous tumor model

The mice were randomly divided into four groups, with five mice in each group. The transfected cells were injected into the flanks of the mice, and tumor size was recorded every 3 days over a continuous period of 4 weeks. The formula for calculating tumor volume is length×width^2/2.

Lung metastasis model

Each group consists of five nude mice, with each mouse receiving a tail vein injection of approximately 1×10^6 transfected cells. In the 4th week, the mice were euthanized to collect their lungs for subsequent analysis.

Orthotopic tumor transplantation model

Tumors derived from subcutaneous tissues induced by Hepa1-6 cells were minced into 2 mm^3 cubes, which were then transplanted into the livers of C57BL/6 mice. For the macrophage clearance experiment, 200 µL of clodronate liposomes (Yeasen, Shanghai, China) were administered via tail vein injection two times a week. After a 4-week period, the intensity and distribution of fluorescence were assessed, and the liver was analyzed.

Primary hepatocellular carcinoma induction assay

Male C57BL/6 mice were divided into two groups, with 25 mice in each group. On the 14th day after birth, the mice received a single intraperitoneal injection of diethylnitrosamine (Sigma) at a concentration of 25 µg/g body weight. Adeno-associated virus serotype 8 vectors carrying the RCOR2 gene or a control sequence (HanBio, Shanghai, China) were injected into the tail vein of each mouse at a dose of 4×10^{10} gene copies per mouse. 4 weeks after the initial administration, the mice were intraperitoneally injected with CCl_4 at a dose of 0.5 µL/g body weight, two times a week, for a total duration of 10 weeks. 48 hours after the final injection, 10 mice from each group were euthanized. The survival of the mice was monitored, and the remaining survival time was recorded with a cut-off at 12 weeks.

PD-1 treatment

The subcutaneous tumor mice, consisting of five mice per group, and the orthotopic tumor mice, comprising five mice per group, were randomly assigned to different groups and subjected to Hepa1-6 cell injection or transplantation. Treatment method: intraperitoneal injection of 200 µg of anti-PD-1 antibody (Bio X Cell, New Hampshire, USA) or anti-IgG antibody (Bio X Cell) was administered every 3 days. Subcutaneous tumor growth was monitored every 3 days, and after 4 weeks, all subcutaneous and orthotopic tumor mice were euthanized.

TCGA cell type identification

CIBERSORT (Cell-type Identification by Estimating Relative Subsets of RNA Transcripts) analysis was used to compare the differences in various immune cell

populations. Additionally, Spearman correlation analysis was performed to investigate the associations between risk factors. The ggplot2 package was employed to visualize the differences in immune cell abundance and the results of the correlation analysis.

Single-cell analysis of single-cell RNA-sequencing (scRNA-seq) data

Download the HCC single-cell RNA-seq dataset GSE202642 from the GEO database.[20] Calculate the percentages of mitochondrial and ribosomal RNA using the "PercentageFeatureSet" function. Use the "FindVariableFeatures" function to select the top 2000 highly variable genes. Scale all genes using the "ScaleData" function. Conduct principal component analysis (PCA) for dimensionality reduction with the "RunPCA" function. Identify cell clusters through the "FindNeighbors" and "FindClusters" functions. Select the top 50 principal components and further reduce dimensions using the Uniform Manifold Approximation and Projection (UMAP) method. Use the "FindAllMarkers" function to filter marker genes for 25 subgroups, setting the log fold change to 0.5 and the minimum expression proportion (minPct) to 0.35 for differential genes. Finally, filter marker genes based on a corrected p value<0.05.

Multiplex immunofluorescence assay

For multiplex immunofluorescence, the sections are dewaxed in xylene, rehydrated in ethanol, and subjected to antigen retrieval using citrate buffer, followed by blocking with 5% BSA. The primary antibody is incubated at 37°C for 60 min, after which the sections are incubated with the corresponding secondary antibody conjugated to horseradish peroxidase. Finally, the cell nuclei are stained with DAPI.

Mass cytometry

An orthotopic tumor transplantation model was established in C57BL/6 mice using Hepa1-6 cells that overexpress RCOR2, along with negative control cells. The transplanted tumors were excised and placed in a tissue preservation solution. Mass cytometry (CyTOF) was subsequently performed by PLTTECH (Hangzhou, China).

Co-immunoprecipitation assay

Use biotin-affinity agarose beads (Beyotime) for the co-immunoprecipitation (Co-IP) assay. Incubate the HCC cell lysate with the antibody overnight at 4°C. Afterward, add the agarose beads and incubate for an additional 2 hours. Wash the agarose beads five times with PBS and extract the protein using RIPA buffer.

For tagged proteins, immunoprecipitation (IP) detection was performed using Anti-His Magnetic Beads and Anti-HA Magnetic Beads (MedChemExpress, New Jersey, USA). The cell lysate, which had been transfected with tagged proteins, was incubated with the corresponding magnetic beads at 4°C for 2 hours with continuous rotation. After washing five times with wash buffer, the proteins were eluted using elution buffer. Western blotting was employed to detect the IP products.

Silver staining assay and mass spectrometry analysis

The Co-IP products from HCC cells, using anti-IgG and anti-RCOR2, were subjected to separate electrophoresis. Following the established protocol, a silver staining reagent kit (Beyotime) was used for the rapid silver staining of the gel strips. Mass spectrometry (MS) performed by the conducted by the Beijing Genomics Institute (Guangzhou, China).

NTA-Ni pull-down assay

Use BeyoMag His-tagged protein purification agarose magnetic beads (Beyotime) for NTA-Ni pull-down experiments. Begin by lysing the cells that have been transfected with the His-tagged protein. Next, add the NTA-Ni magnetic beads and incubate the mixture at 4°C with rotation for 1 hour. Afterward, wash the beads three times with wash buffer, then add elution buffer to elute the protein. Finally, detect the isolated purified His-tagged protein using western blot analysis.

Ubiquitination detection assay

Treat the transfected cells with 20 µM MG132 (Beyotime) for 6 hours. Subsequently, collect the total protein. Isolate the supernatant and perform IP using anti-HA magnetic beads. After eluting the protein, assess the ubiquitination level of RCOR2 using either a ubiquitin antibody or a His-ubi antibody.

Immunofluorescence assay

After fixing the cells cultured in a confocal dish with formaldehyde, permeabilize them with 0.5% Triton X-100 for 10 min. Next, add the primary antibody specific to the target protein and incubate overnight. Following this, stain the cells with a fluorescently labeled secondary antibody. DAPI is used to label the cell nuclei, and cell morphology is observed using a laser confocal microscope (Olympus).

Subcellular fractionation assays

According to the recommended protocol, use a Subcellular Fractionation Kit (Invitrogen) for the subcellular separation experiment. In summary, add the fractionation buffer to the cells and incubate on ice for 10 min. Subsequently, centrifuge the mixture at 500 g at 4°C for 5 min to separate the cytoplasm from the nucleus. Next, combine the nuclear fraction with cell lysis buffer and vortex for 5 min. After adding loading buffer to both the cytoplasmic and nuclear fractions, boil the samples for 10 min before conducting a western blot to detect protein distribution between the nucleus and cytoplasm.

Statistical analysis

The experimental data were analyzed using SPSS V.22.0 (IBM, SPSS, Chicago, Illinois, USA) and GraphPad Prism V.9.0 (GraphPad, San Diego, California, USA). Differences in means were assessed using the Student's t-test or

one-way analysis of variance, followed by Tukey's honestly significant difference post hoc test when the assumptions of normality and equal variance were satisfied. The analysis of clinical features was conducted using the χ^2 test, while correlation assessments were performed using Spearman correlation analysis. Survival curves were generated using the Kaplan-Meier method. Both univariate and multivariate analyses were executed using the Cox proportional hazards model. Bar graphs are presented as the mean±SD. The following significance levels were used: ns, not significant; *p<0.05, **p<0.01, ***p<0.001.

RESULTS

The hypoxia-related factor RCOR2 is a critical gene associated with poor prognosis and inhibits the infiltration of CD8+ T cells in HCC

To investigate hypoxia-related genes in HCC, Huh7 and YY8103 cells were cultured in a hypoxic incubator with 1% O_2 for 48 hours. Subsequently, a comparative gene analysis was conducted between hypoxic and normoxic cells using high-throughput sequencing technology (figure 1A). Additionally, the infiltration levels of 29 immune cell types in 374 liver cancer sequencing samples from the the Cancer Genome Atlas (TCGA) database were quantified using single-sample Gene Set Enrichment Analysis (GSEA) (figure 1B). Based on the distribution levels of CD8+T cells, the samples were categorized into high and low infiltration groups, from which differential genes were identified. By integrating hypoxia-related genes in HCC cells with the differential genes of $CD8^+$ T cells, four genes were identified as upregulated in hypoxic HCC cells and inversely correlated with $CD8^+$ T-cell infiltration (figure 1C). Subsequently, we categorized the HCC samples from TCGA into hypoxic and normoxic groups based on hypoxia-related indicators. Expression analyses revealed that RCOR2 was significantly upregulated in hypoxic HCC tissues (online supplemental figure S1A). Furthermore, survival analyses indicated that patients with high RCOR2 expression in the hypoxic group exhibited a markedly lower overall survival time compared with those in other groups (online supplemental figure S1B). The detection of RCOR2 expression in both hypoxic and normoxic cells further corroborated that RCOR2 is upregulated under hypoxic conditions (online supplemental figure S1C,D). Consequently, RCOR2 was selected for further investigation.

The analysis of TCGA data revealed an upregulation of RCOR2 in HCC, which was positively correlated with the staging of HCC tissues (figure 1D and E). Survival analysis indicated that patients with HCC with elevated RCOR2 expression exhibited decreased overall and disease-free survival times (figure 1F and G). We further investigated the expression of RCOR2 and its clinical relevance in 80 pairs of HCC tissues and adjacent non-tumor tissues. The study revealed upregulation of RCOR2 in HCC tissues through qRT-PCR and western blot assays (figure 1H and I). Clinical data analysis revealed a correlation between RCOR2 expression, HCC tissue size, microvascular infiltration, and stage (table 1). High RCOR2 expression was associated with reduced overall survival time in patients with HCC (figure 1J). Multivariate logistic regression analysis identified RCOR2 as an independent predictor of overall survival (figure 1K). The staining results from the TMAs indicate that RCOR2 is upregulated in HCC and is associated with a reduction in $CD8^+$ T-cell infiltration (figure 1L–M). In summary, the hypoxia-related factor RCOR2 is a critical gene associated with poor prognosis in HCC and the suppression of $CD8^+$ T-cell infiltration.

RCOR2 promotes the proliferation and metastasis of HCC cells under hypoxic conditions

To investigate the regulatory role of RCOR2 in the function of HCC cells, we established RCOR2 knockdown HCC cell lines in Huh7 cells, which exhibit high RCOR2 expression, and RCOR2-overexpressing HCC cell lines in Hep3B cells, which have low RCOR2 expression (online supplemental figures 2A–C). CCK-8, EdU, colony formation, and transwell assays demonstrated that the overexpression of RCOR2 significantly enhanced the proliferation, migration, and invasion capabilities of Hep3B cells (figure 2A–D). We further examined the regulatory role of RCOR2 in HCC cells under hypoxic conditions. The results indicated that hypoxia increased the proliferation, migration, and invasion abilities of Huh7 cells. Conversely, the knockdown of RCOR2 inhibited the enhancing effects of hypoxic conditions on the proliferation, migration, and invasion of Huh7 cells (figure 2E–H). Additionally, a nude mouse subcutaneous tumor model and a lung metastasis model further confirmed that RCOR2 promotes the proliferation and metastasis of HCC cells in vivo (figure 2I–J). In conclusion, the results presented above indicate that RCOR2 can promote the proliferation and metastasis of HCC cells under both normoxic and hypoxic conditions.

RCOR2 promotes the glycolytic process in HCC cells

To investigate the regulatory mechanism of RCOR2 in the progression of HCC cells, we conducted RNA high-throughput sequencing analysis on Hep3B-NC and Hep3B-RCOR2 cells (figure 3A). The results from Gene Ontology (GO) and Kyoto Encyclopedia of Genes and Genomes pathway enrichment analyses indicated that RCOR2 is implicated in several metabolic processes, including the tricarboxylic acid cycle, glycolysis, pyruvate metabolism, and ATP metabolism (figure 3B–C). Additionally, GSEA revealed that RCOR2 enhances glycolysis and ATP metabolism (figure 3D). To investigate the role of RCOR2 in the regulation of glycolysis in HCC cells, we measured lactate production, glucose uptake, and ATP synthesis. The findings indicated that the overexpression of RCOR2 resulted in increased lactate production, enhanced glucose uptake, and elevated ATP synthesis in HCC cells (figure 3E). Furthermore, we assessed the ECAR and OCR of HCC cells. The results from the ECAR analysis indicate that the overexpression

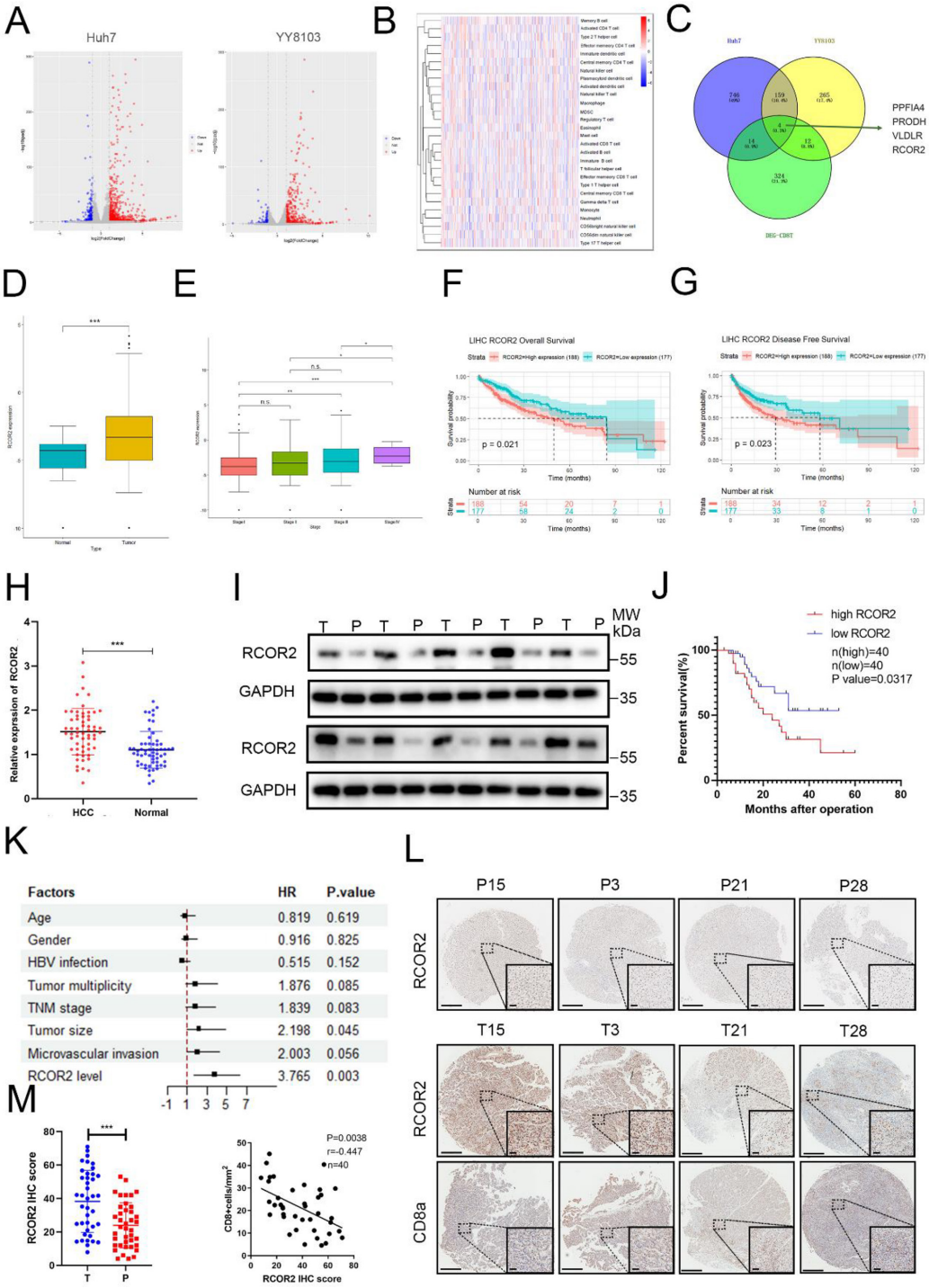

Figure 1 The hypoxia-related factor RCOR2 is a critical gene associated with poor prognosis and inhibits the infiltration of CD8$^+$ T cells in HCC. (A) Volcano plots illustrate the results of high-throughput sequencing conducted on Huh7 and YY8103 cell lines cultured under normoxic or hypoxic conditions. (B) The infiltration levels of 29 immune cell types in 374 HCC sequencing samples from the TCGA database. (C) The Venn diagram illustrates proteins associated with hypoxia-induced responses and CD8$^+$ T-cell infiltration. (D) Analysis of The TCGA data indicates that RCOR2 is significantly upregulated in HCC. (E) An analysis of TCGA data reveals a positive correlation between RCOR2 expression and the staging of HCC tissues. (F–G) Survival analysis indicated that patients with HCC with elevated RCOR2 expression exhibited decreased overall (F) and disease-free survival times (G). (H–I) The quantitative real-time PCR (H) and western blot (I) results indicate that RCOR2 is upregulated in HCC tissues (T: HCC tissue, P: para-carcinoma tissue). (J) Survival analysis indicates that patients exhibiting elevated levels of RCOR2 expression experience a reduced overall survival duration. (K) Forest plot showing the results of multivariate analysis of factors associated with OS. (L–M) IHC staining was used to detect RCOR2 expression and CD8$^+$ T-cell infiltration in HCC tissues (T: HCC tissue, P: para-carcinoma tissue). Scale bar: 200 µm and 50 µm. Bar graphs represent mean±SEM (n=3, *p<0.05, **p<0.01, and ***p<0.001). HBV, hepatitis B virus; HCC, hepatocellular carcinoma; IHC, immunohistochemistry; OS, overall survival; RCOR2, REST corepressor 2; TCGA, the Cancer Genome Atlas; TNM, tumor, node, metastasis.

Table 1 Correlation between RCOR2 expression and clinicopathological features

Clinicopathological features	All cases		RCOR2		P *value*
			High expression	Low expression	
Age (years)	>60	59	31	28	
	≤60	21	9	12	0.6120
Gender	Female	35	17	18	0.7257
	Male	45	23	22	
HBV	Negative	12	7	5	
	Positive	68	33	35	0.5888
Tumor multiplicity	Single	57	24	33	
	Multiple	23	16	7	**0.0469***
Tumor size (cm)	≤5	49	17	32	
	>5	31	23	**8**	**0.0011****
α-fetoprotein (ng/mL)	≤200	19	9	10	
	>200	61	31	30	0.8217
Edmondson stage	I-II	55	22	33	
	III-IV	25	18	7	**0.0150***
TNM stage	I	48	19	29	
	II-III	32	21	**11**	**0.0392***
Microvascular invasion	Yes	27	20	7	
	No	53	20	33	**0.0041****

*p<0.05, **p<0.01.
P-values in bold indicate statistical significance.
HBV, hepatitis B virus; RCOR2, REST corepressor 2; TNM, tumor, node, metastasis.

of RCOR2 enhances both the glycolytic rate and glycolytic capacity of HCC cells (figure 3F). Additionally, the results from the OCR measurements indicate that the overexpression of RCOR2 is associated with a decrease in both basal respiration and maximum respiration in HCC cells (figure 3G). We further investigated the regulatory role of RCOR2 in glycolysis within HCC cells under hypoxic conditions. The results demonstrated that hypoxia increased lactate production, glucose uptake, and ATP synthesis in HCC cells. However, the knockdown of RCOR2 inhibited the enhancing effects of hypoxia on these metabolic functions (figure 3H). Additionally, the results from the ECAR and OCR assays indicated that hypoxia elevated the glycolytic rate in HCC cells while simultaneously suppressing their respiratory function; however, the knockdown of RCOR2 mitigated these effects (figure 3I–J). Finally, we investigated the regulatory role of RCOR2 in the glycolysis of HCC cells in vivo by employing immunohistochemical detection of subcutaneous tumors in mice. The results demonstrated that RCOR2 promotes the expression of GLUT1, HK2, and LDHA, indicating that RCOR2 enhances glycolysis in HCC in vivo (online supplemental figure 2D). Collectively, these experiments suggest that RCOR2 plays a crucial role in providing energy to HCC cells by enhancing glycolysis under hypoxic conditions.

RCOR2 induces an inhibitory tumor immune microenvironment

To investigate the regulatory function of RCOR2 within the immune microenvironment of HCC, we stratified the samples into RCOR2 high risk and RCOR2 low risk categories based on the median expression levels of RCOR2 derived from 374 HCC sequencing samples in TCGA. Immune cell infiltration analysis revealed a negative correlation between RCOR2 expression and $CD8^+$ T-cell infiltration, while a positive correlation was observed with M2 macrophage polarization (online supplemental figure S3A). Furthermore, an examination of molecules associated with $CD8^+$ T-cell functionality indicated that RCOR2 expression was linked to the functional exhaustion of $CD8^+$ T cells (online supplemental figure S3B). Additionally, we conducted a clustering analysis of single-cell sequencing data from seven HCC samples obtained from the GEO database (GSE202642) (online supplemental figure S2C). We focused on samples 5 and 7, which exhibited significant differences in RCOR2 expression levels (online supplemental figure S2D). The UMAP plot illustrated the distribution of subpopulations between these samples (online supplemental figure S2E). We observed that the proportion of PD-1, lymphocyte-activation gene 3 (LAG-3), and CTLA-4 positive $CD8^+$ T cells was elevated in samples with high RCOR2 expression, while the proportion of GzmB positive cells was decreased. Additionally, the proportion of CD163 positive macrophages

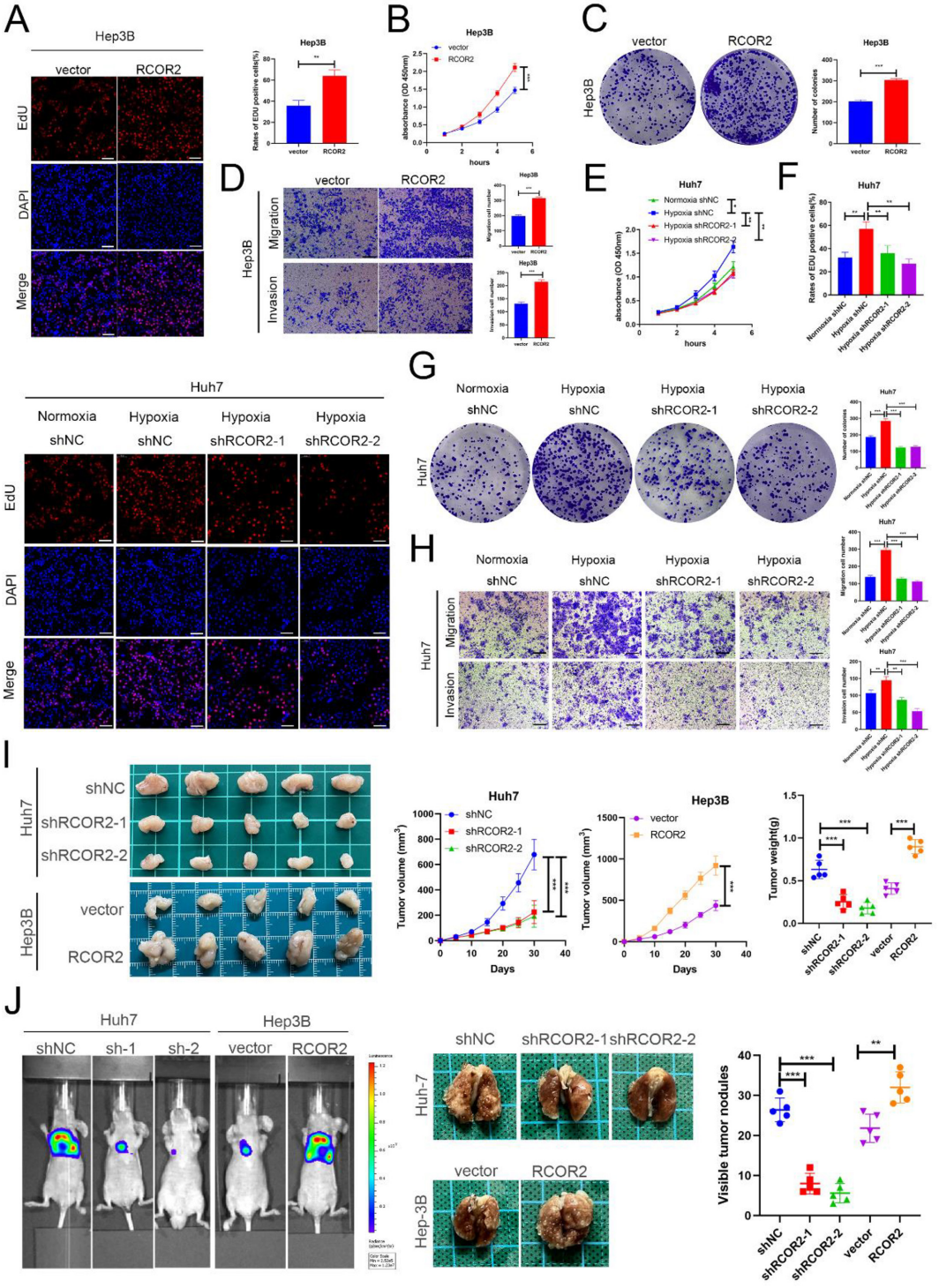

Figure 2 RCOR2 promotes the proliferation and metastasis of HCC cells under hypoxic conditions. (A–C) EdU (A), CCK-8 (B), and colony formation (C) assays indicated that the overexpression of RCOR2 promoted the proliferation of HCC cells. Scale bar: 50 µm. (D) Transwell assay demonstrated that the overexpression of RCOR2 enhanced the migration and invasion of HCC cells. Scale bar: 200 µm. (E–G) The CCK8 (E), EdU (F), and colony formation (G) experiments indicate that the knockdown of RCOR2 inhibits the stimulatory effect of hypoxia on the proliferation of HCC cells. Scale bar: 50 µm. (H) The transwell experiment demonstrated that the knockdown of RCOR2 inhibited the enhancing effect of hypoxia on the migration and invasion of HCC cells. Scale bar: 200 µm. (I) A subcutaneous tumor model was utilized to detect the proliferation of RCOR2-deficient Huh7 cells and RCOR2-overexpressing Hep3B cells in vivo. Photograph of subcutaneous tumors (left), growth curve of subcutaneous tumors (middle), and weight of subcutaneous tumors (right). (J) A lung metastasis model was generated to detect the metastasis of HCC cells. In vivo image of nude mice (left), representative images of lungs (middle), and number of visible tumor nodules (right). Bar graphs represent mean±SEM (n=3, *p<0.05, **p<0.01, and ***p<0.001). DAPI, 4',6-diamidino-2-phenylindole; EdU, 5-ethynyl-20-deoxyuridine; CCK-8, cell counting kit-8; HCC, hepatocellular carcinoma; RCOR2, REST corepressor 2.

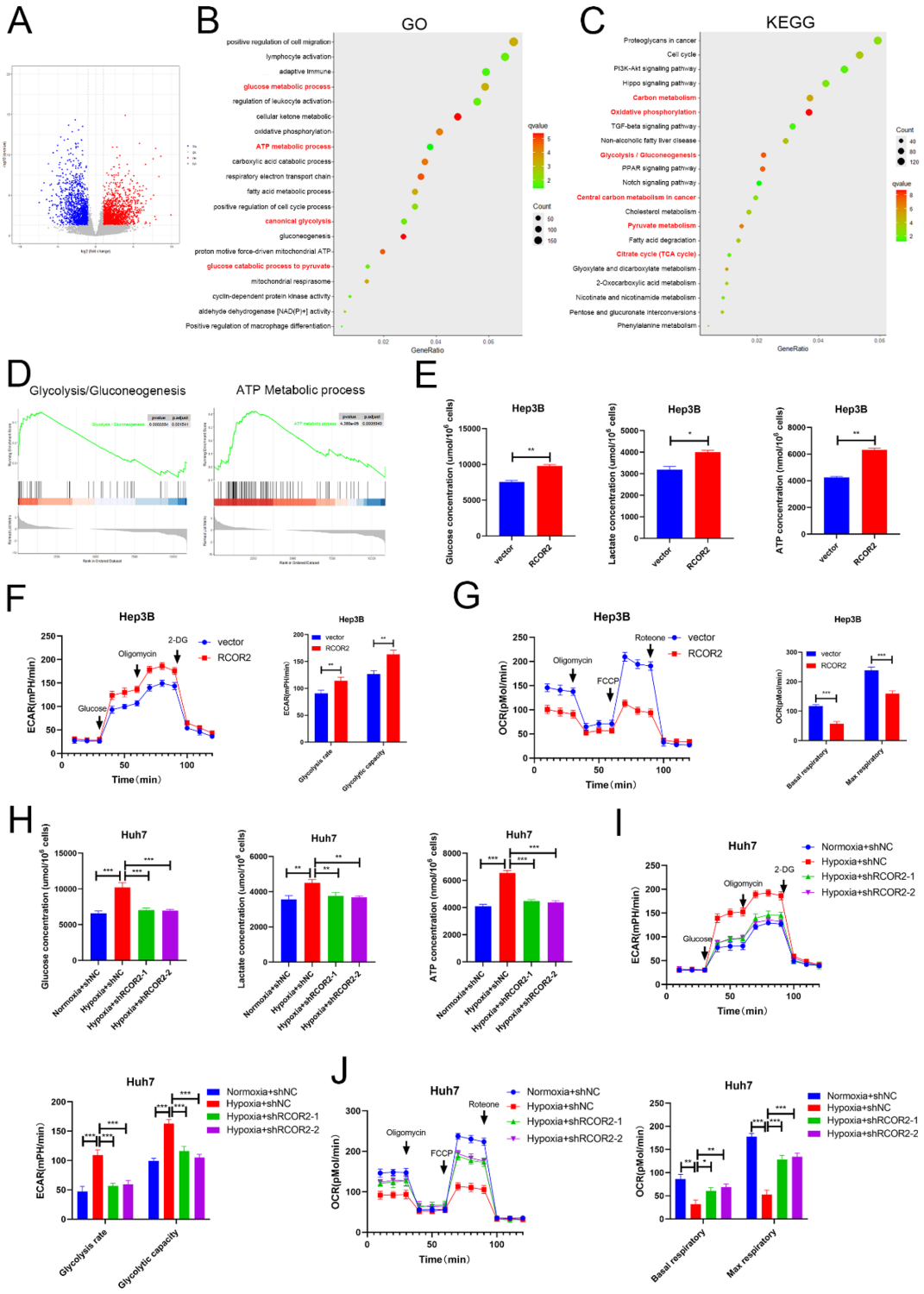

Figure 3 RCOR2 promotes the glycolytic process in hepatocellular carcinoma cells. (A) The RNA-seq volcano map of three pairs of RCOR2-overexpressing Hep3B cells and negative control cells. (B–C) GO enrichment analysis (B) and KEGG pathway analysis (C) of the RNA-seq results. (D) Gene Set Enrichment Analysis analysis of subsets of genes related to the glycolysis and ATP metabolic process. (E) The glucose consumption, lactate production, and ATP levels were measured in Hep3B cells overexpressing RCOR2. (F) The analysis of ECAR in Hep3B cells overexpressing RCOR2. ECAR levels after glucose injection reflect glycolysis rate, while ECAR levels after oligomycin injection reflect glycolytic capacity. (G) The analysis of OCR in Hep3B cells overexpressing RCOR2. OCR measured before oligomycin injection represents the basal respiratory rate, while OCR measured after FCCP injection represents the maximum respiratory rate. (H) The glucose consumption, lactate production, and ATP levels of Huh7 cells were measured under normoxic and hypoxic conditions. (I–J) The analysis of ECAR and OCR in Huh7 cells under hypoxic conditions. Bar graphs represent mean±SEM (n=3, *p<0.05, **p<0.01, and ***p<0.001). ECAR, extracellular acidification rate; FCCP, fluoro-carbonyl cyanide phenylhydrazone; GO, Gene Ontology; KEGG, Kyoto Encyclopedia of Genes and Genomes; OCR, oxygen consumption rate; RCOR2, REST corepressor 2; RNA-seq, RNA sequencing.

was increased (online supplemental figures S2F and G). These findings suggest that RCOR2 may play a role in regulating macrophage M2 polarization and the functional exhaustion of $CD8^+$ T cells.

To investigate the regulatory role of RCOR2 in the immune microenvironment of HCC, we established an orthotopic tumor transplantation model. In this model, tumor volume was significantly increased in the RCOR2 overexpression group (figure 4A–B). The results of CyTOF testing on orthotopic tumors indicated that in the RCOR2 overexpression group, the proportion of $CD8^+$ T-cell infiltration was reduced, while the expression of exhaustion markers CD279 and CD39 was upregulated. Additionally, in the RCOR2 overexpression group, the surface expression of CD163 on macrophages was also upregulated (figure 4D–G), suggesting that RCOR2 promotes M2-type polarization of macrophages. Further multicolor immunofluorescence experiments revealed that in the RCOR2 overexpression group, $CD8^+$ T-cell infiltration was downregulated, while the proportion of M2 macrophage infiltration was upregulated (figure 4H). Furthermore, we established a primary HCC induction assay in mice. We used AAV 8 to achieve targeted overexpression of RCOR2 in the hepatic tissue of the mice (figure 4I–J). Our findings revealed a significantly higher incidence of tumors, larger tumor sizes, and an increased number of tumor lesions in the RCOR2 overexpression group compared with the control group (figure 4K). Survival analysis showed that the control group had a longer overall survival than the RCOR2 overexpression group (figure 4L). Immunohistochemical analyses indicated an increased infiltration of macrophages in the RCOR2 overexpression group, while the infiltration of $CD8^+$ T cells was reduced (figure 4M). Flow cytometric analysis of non-parenchymal tumor cells confirmed an upregulation of macrophage populations in the RCOR2 overexpression group, accompanied by an increase in CD206-positive macrophages. Conversely, the proportion of $CD8^+$ T cells decreased, while the number of PD-1-positive and CTLA-4-positive $CD8^+$ T cells increased, accompanied by a reduction in GzmB-positive cells (figure 4N–Q, (online supplemental figure S4A). These findings suggest that RCOR2 promotes the M2 polarization of TAMs in vivo and contributes to the functional exhaustion of $CD8^+$ T cells.

RCOR2 promotes $CD8^+$ T-cell functional exhaustion by inducing M2 polarization of macrophages

To investigate the regulatory function of RCOR2 in the functional exhaustion of $CD8^+$ T cells, we isolated $CD8^+$ T cells from human PBMCs and activated them. Subsequently, we co-cultured them with HCC cells. Flow cytometry analyses revealed that neither the knockdown nor the overexpression of RCOR2 had a direct impact on the expression levels of exhaustion markers on the surface of $CD8^+$ T cells (online supplemental figures S5A and B). Next, we used PMA to induce the differentiation of THP-1 cells into macrophages, which were then co-cultured with HCC cells (figure 5A, online supplemental figure S5C). Following co-culture with HCC cells that overexpressed RCOR2, macrophages exhibited elevated levels of the membrane proteins CD206 and CD163, along with increased messenger RNA expression of CD206, ARG-1, IL-10, and transforming growth factor-β (TGF-β), as well as enhanced production of IL-10 and TGF-β. Conversely, these effects were diminished in the RCOR2 knockdown group (figure 5B–G), suggesting that RCOR2 facilitates the M2 polarization of macrophages. Previous studies have established a close relationship between TAMs and the functionality of $CD8^+$ T cells. In addition to inhibiting $CD8^+$ T cells via programmed cell death 1 ligand 1 (PD-L1)/PD-1 interactions, TAMs can also secrete immunosuppressive cytokines and enzymes. Consequently, we hypothesize that RCOR2 may suppress $CD8^+$ T-cell activity by promoting the M2 polarization of macrophages. To elucidate this mechanism, we established a co-culture model comprising macrophages co-cultured with HCC cells and $CD8^+$ T cells (online supplemental figure S5D). The results of flow cytometry showed that in the RCOR2 knockdown group, the level of PD-1 and CTLA-4 on $CD8^+$ T cells decreased while the level of GzmB increased, whereas the opposite effect was observed in the RCOR2 overexpression group (figure 5H–J). This suggests that RCOR2 modulates $CD8^+$ T-cell exhaustion through the induction of macrophage polarization. To validate these findings in vivo, we examined whether the depletion of TAMs using clodronate liposomes could counteract the inhibitory effects of RCOR2 overexpression on $CD8^+$ T cells. The results demonstrated that following treatment with clodronate liposomes, macrophages within the tumor no longer expressed, and the disparity in the proportion of $CD8^+$ T cells between tumors of mice with RCOR2 overexpression and the control group was eliminated (figure 5K–N, online supplemental figure S6A). Collectively, these findings indicate that RCOR2 inhibits $CD8^+$ T-cell activity by promoting the M2 polarization of macrophages.

RCOR2 induces macrophage polarization by transcriptionally activating LIF

To elucidate the downstream targets modulated by RCOR2 during macrophage polarization, we analyzed ChIP-sequencing data (ChIP-seq: ENCSR455DOO, controls: ENCSR239QGH) for RCOR2 obtained from HCC cells (figure 6A–B).[21 22] Through de novo motif analysis, we identified a motif that exhibited a strong correlation with RCOR2 occupancy (figure 6C). By integrating the downstream RNA-seq data with the ChIP-seq data for RCOR2, we identified a total of 425 genes (figure 6D). GO enrichment analysis of the RNA-seq data revealed that the intersecting genes are associated with the regulation of macrophage differentiation, and these genes are presented in a heatmap format (figure 6E). Among them, cytokines LIF and MMP9 were enriched in both RNA-seq and ChIP-seq analyses. Correlation analysis using the TCGA data indicated that LIF exhibited the strongest correlation with RCOR2 (online supplemental figure

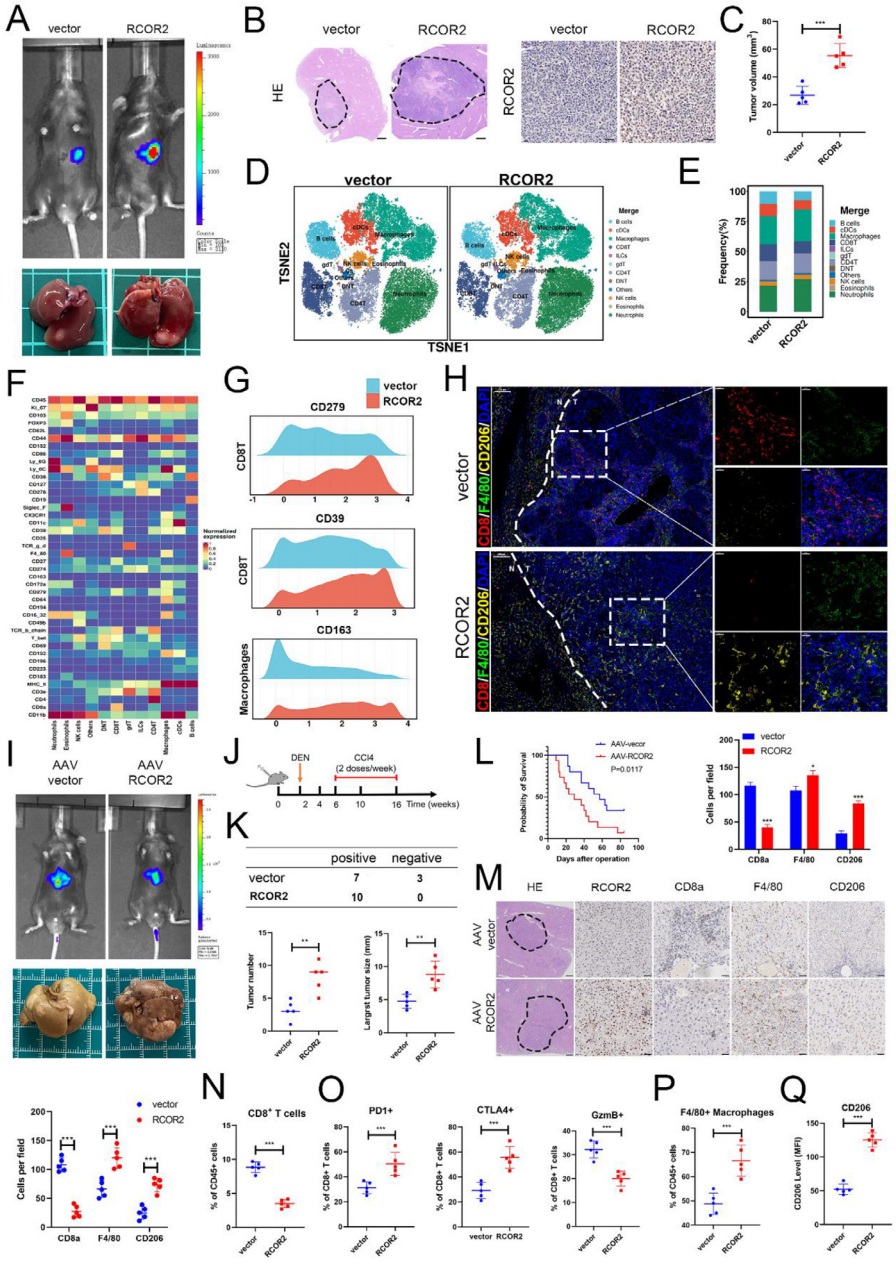

Figure 4 RCOR2 induces an inhibitory tumor immune microenvironment. (A) An orthotopic xenograft model was established in C57BL/6 mice. The lentivirus carrying a luciferase tag is shown in the in vivo images of the mice (above), along with representative images of the livers (below). (B) Immunohistochemistry of H&E, RCOR2 in orthotopic tumors. Scale bars: 200 µm and 50 µm. (C) The volume of orthotopic tumors. (D) T-SNE analysis of mass cytometry data of immune cells from orthotopic tumor tissues. (E) Comparative abundance of the tumor microenvironment in control versus RCOR2-overexpression orthotopic tumors. (F) The heatmap showing the expression of target proteins in all 12 subclusters. (G) Analyzing the density of CD279 and CD39 in CD8$^+$ T cells, as well as the density of CD163 in macrophages. (H) Representative images from multiplex immunofluorescence analysis of CD8, F4/80, and CD206 markers in orthotopic tumors. Scale bars: 100 µm and 50 µm. (I) AAV-8 carrying the RCOR2 overexpression plasmid and luciferase tag was administered to mice via tail vein injection. In vivo image of mice (above), representative images of livers (below). (J) Workflow of the spontaneous HCC model. (K) The proportion of tumor positivity, tumor count, and maximum tumor volume were compared between the RCOR2 overexpression group and the control group in the spontaneous HCC model. (L) Survival analysis of RCOR2 overexpression in comparison to the control group in a spontaneous HCC model. (M) Immunohistochemistry of H&E, CD8a, F4/80, and CD206 in spontaneous tumors. Scale bars: 200 µm and 50 µm. (N) Flow cytometry analysis of the percentage of CD8$^+$ T cells in CD45+TILs from spontaneous tumors. (O) Flow cytometry analysis of PD-1+, CTLA-4+, and GzmB+ (I) in CD8+T cells from spontaneous tumors. (P) Flow cytometry analysis of the percentage of macrophages in CD45+TILs from spontaneous tumors. (Q) Flow cytometry analysis of CD206+in macrophages from spontaneous tumors. Bar graphs represent mean±SEM (**p<0.01, and ***p<0.001). AAV-8, adeno-associated virus serotype 8; CTLA-4, cytotoxic T-lymphocyte associated protein 4; DEN, diethylnitrosamine; GzmB, granzyme B; HCC, hepatocellular carcinoma; PD-1, programmed cell death protein 1; RCOR2, REST corepressor 2; TILs, tumor-infiltrating lymphocytes; T-SNE, t-distributed stochastic neighbor embedding.

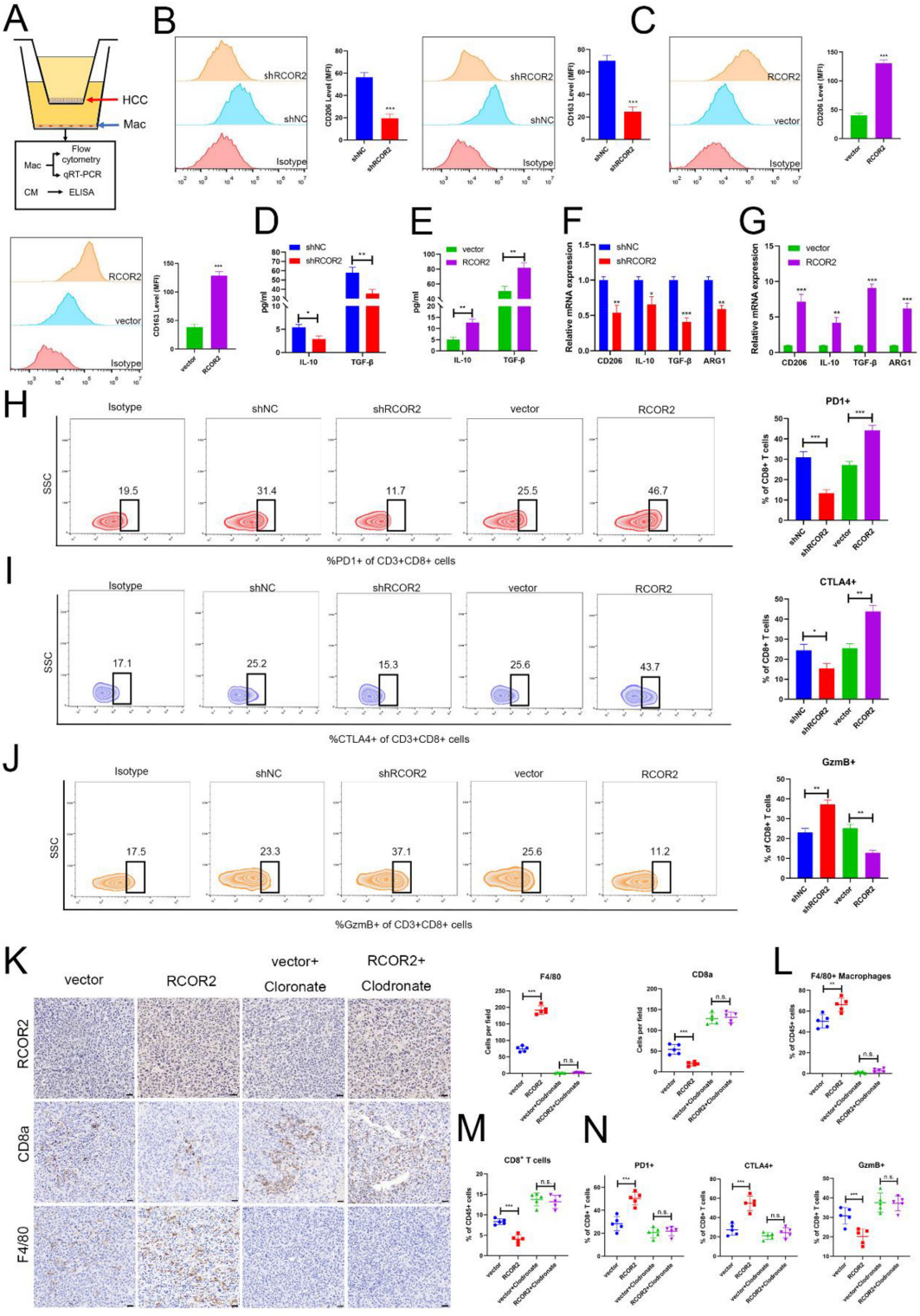

Figure 5 RCOR2 promotes CD8+T cell functional exhaustion by inducing M2 polarization of macrophages. (A) Schematic diagram showing HCC cells co-cultured with macrophages. (B–C) CD163 and CD206 expression in macrophages detected by flow cytometry. (D–E) Secreted IL-10 and TGF-β in the supernatants of macrophages detected by ELISA. (F–G) CD206, IL-10, and TGF-β messenger RNA levels in macrophages detected by qRT-PCR. (H–J) Flow cytometry analysis of the percentage of PD-1+ (H), CTLA-4+ (I), and GzmB+ (J) in $CD8^+$ T cells. (K) Immunohistochemistry of RCOR2, CD8a, and F4/80 in orthotopic tumors. Scale bar: 50 µm. (L–M) Flow cytometry analysis of the percentage of $CD8^+$T cells (L), and macrophages (M) in $CD45^+$ TILs from orthotopic tumors. (N) Flow cytometry analysis of the percentage of PD-1+, CTLA4+, and GzmB+ in $CD8^+$ T cells from orthotopic tumors. Bar graphs represent mean±SEM (n=3, *p<0.05, **p<0.01, and ***p<0.001). CTLA-4, cytotoxic T-lymphocyte associated protein 4; GzmB, granzyme B; HCC, hepatocellular carcinoma; IL, interleukin; PD-1, programmed cell death protein 1; qRT-PCR, quantitative real-time PCR; RCOR2, REST corepressor 2,TGF, transforming growth factor; TILs, tumor-infiltrating lymphocytes.

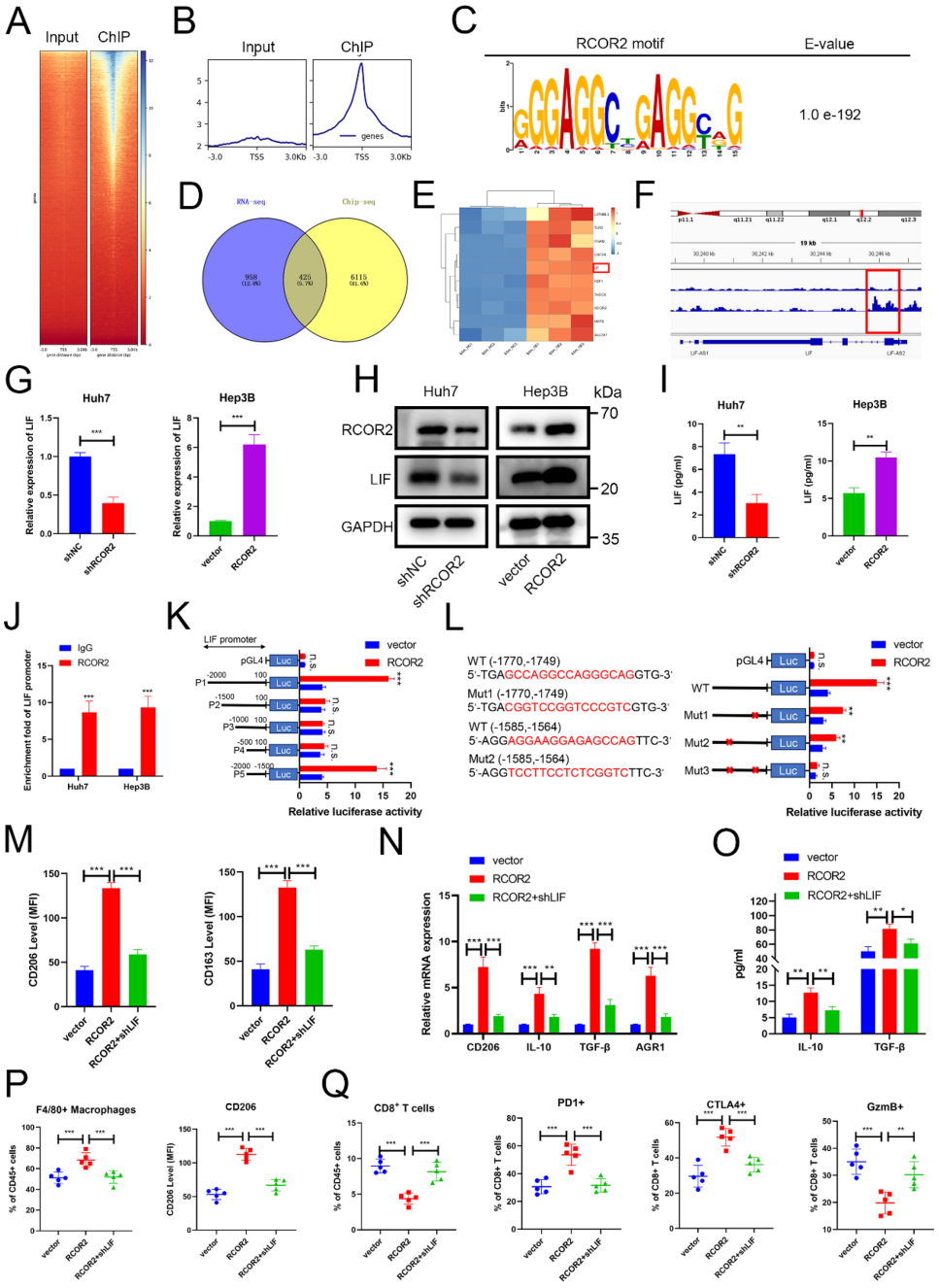

Figure 6 RCOR2 induces macrophage polarization by transcriptionally activating LIF. (A–B) Density plot showing the ChIP-sequencing result of high-confidence RCOR2 peaks, ranked by intensity. (C) The de novo motif logo of RCOR2 was derived from ChIP-sequencing data. (D) Venn diagram of overlapping genes between ChIP-sequencing and RNA-sequencing. (E) A heatmap illustrating the genes involved in macrophage differentiation, with genes identified in ChIP-sequencing analyses and RNA-seq analyses. (F) Enrichment of RCOR2 in the promoter region of LIF according to ChIP-sequencing. (G–I) qRT-PCR (G), western blot (H), and ELISA (I) were used for detecting LIF expression. (J) The ChIP experiment demonstrates that the LIF promoter fragment can be enriched by anti-RCOR2 antibodies. (K) Relative luciferase activities of reporters containing full-length or fragments of the LIF promoter. (L) Relative luciferase activities of different reporters containing wild type (WT) and mutated (Mut) sequences of the LIF promoter in the indicated cells. (M) Quantification of CD163 and CD206 expression in macrophages using flow cytometry analysis. (N) CD206, IL-10, TGF-β, and AGR1 mRNA levels in macrophages, detected by qRT-PCR analyses. (O) Secreted IL-10 and TGF-β in macrophage supernatants, detected using ELISA. (P) Flow cytometry analysis of the percentage of macrophages in $CD45^+$ TILs, and CD206+ in macrophages from orthotopic tumors. (Q) Flow cytometry analysis of the percentage of $CD8^+$ T cells in $CD45^+$ TILs, PD-1+, CTLA-4+, and GzmB+ in $CD8^+$ T cells from orthotopic tumors. Bar graphs represent mean±SEM (n=3, *p<0.05, **p<0.01, and ***p<0.001). ChIP, chromatin immunoprecipitation; CTLA-4, cytotoxic T-lymphocyte associated protein 4; GzmB, granzyme B; IL, interleukin; LIF, leukemia inhibitory factor; MFI, mean fluorescence intensity; mRNA, messenger RNA; PD-1, programmed cell death protein 1; qRT-PCR, quantitative real-time PCR; RCOR2, REST corepressor 2; RNA-seq, RNA sequencing; TGF, transforming growth factor; TILs, tumor-infiltrating lymphocytes.

S7A). In addition, survival analysis of TCGA data indicates that LIF is associated with the prognosis of patients with HCC (online supplemental figure S7B). Consequently, we hypothesize that LIF may serve as a critical target for RCOR2 in the regulation of macrophage polarization. qRT-PCR and western blot analyses revealed that the overexpression of RCOR2 enhances LIF expression, whereas the knockdown of RCOR2 results in a reduction of LIF expression (figure 6G–H). ELISA results indicated that RCOR2 overexpression promotes LIF secretion by HCC cells, while the opposite effect was observed following RCOR2 knockdown (figure 6I). Based on the peak fragment sequences of RCOR2 enriched in the LIF promoter region from the ChIP-seq results, we designed ChIP-quantitative PCR primers for LIF. ChIP experiments have demonstrated that RCOR2 can bind to fragments of the LIF promoter (figure 6J). Subsequently, we cloned the LIF promoter regions (P1: −2,000 to +100, P2: −1,500 to +100, P3: −1,000 to +100, P4: −500 to +100, and P5: −2,000 to −1,500) into the luciferase reporter plasmid. Fluorescence detection indicating that the −2,000 to −1,500 fragment is used for RCOR2-mediated transcriptional activation (figure 6K). Based on the identified RCOR2 binding motif, we noted that the −2,000 to −1500 fragment contains two putative binding sites for RCOR2. We constructed mutated sequences for both sites and incorporated them into the luciferase reporter plasmid. The luciferase reporter assays indicated that mutations at either site partially diminished the enhancement of RCOR2-mediated LIF promoter activity, while simultaneous mutations at both sites completely abrogated this activity (figure 6L). This indicates that both of these sites can mediate the transcriptional activation of LIF by RCOR2.

Next, we investigated the regulatory effect of LIF on macrophage polarization. Following treatment with human recombinant LIF, the expression levels of CD206 and CD163 on the surface of macrophages were upregulated, and the secretion of IL-10 and TGF-β increased. These findings suggest that exogenous LIF can promote the M2 polarization of macrophages (online supplemental figure S8A–C). Subsequently, we assessed the role of RCOR2 in regulating macrophage polarization through LIF. We constructed lentiviruses for LIF knockdown and overexpression, and verified transfection efficiency using western blot assay (online supplemental figure S8D). In vitro analyses showed that the knockdown of LIF resulted in a decrease in the surface markers CD163 and CD206 in M2 macrophages induced by RCOR2 overexpression, as well as a reduction in the secretion of IL-10 and TGF-β from these macrophages (figure 6M–O). In vivo results demonstrated that the knockdown of LIF attenuated the promoting effect of RCOR2 overexpression on M2 macrophage polarization and countered the impact of RCOR2 overexpression on the functional exhaustion of $CD8^+$ T cells (figure 6P–Q, online supplemental figure S8E–G). These findings suggest that RCOR2 enhances M2 macrophage polarization by increasing the transcriptional activity of LIF.

Hypoxia enhances the SUMOylation of RCOR2 by upregulating PIAS4

Previous studies have demonstrated that HIF1α can enhance the transcription of RCOR2.[17 23] Western blot and qRT-PCR experiments revealed that the knockdown of HIF1α inhibited the stimulatory effect of hypoxia on RCOR2 expression in HCC (online supplemental figure S9A and B). TCGA correlation analysis showed that RCOR2 expression is positively correlated with HIF1α in HCC (online supplemental figure S9C). We further analyzed the binding motifs of HIF1α using the JASPAR database and identified two potential binding sites on the RCOR2 promoter (online supplemental figure S9D–E). Based on these predicted binding sites, we constructed RCOR2 promoter WT and mutant luciferase reporter plasmid. The results of the luciferase reporter assay indicated that the fluorescence intensity decreased in the WT group following HIF1α knockdown, while there was no significant change in the mutant group (online supplemental figure S9F), suggesting that HIF1α can promote the transcription of RCOR2.

Meanwhile, through IP experiments and protein MS analysis, we discovered that the binding affinity of RCOR2 to the ubiquitin-like ligase PIAS4 is enhanced under hypoxic conditions (figure 7A, online supplemental figure S10A). We confirmed the direct interaction between RCOR2 and PIAS4 using both exogenous and endogenous Co-IP methods (figure 7B–C). Immunofluorescence experiments demonstrated that RCOR2 and nuclear PIAS4 co-localize in HCC cells (online supplemental figure S10B). Previous research has shown that the CoREST complex can undergo sumoylation[24]; therefore, we hypothesize that the hypoxic environment plays a role in regulating the sumoylation modification of RCOR2. By transfecting His-tagged SUMO1, SUMO2, SUMO3, FLAG-tagged UBC9, and HA-tagged RCOR2 into Huh7 and Hep3B cells, we observed a protein band with a molecular weight of approximately 80 kDa in the SUMO2 group during the Ni-NTA pull-down experiment, suggesting that RCOR2 can be sumoylated by SUMO2 (figure 7D). We investigated the regulatory role of PIAS4 in the sumoylation of RCOR2. The results indicated that the knockdown of PIAS4 inhibited the sumoylation of RCOR2, whereas the overexpression of PIAS4 enhanced the sumoylation of RCOR2 (figure 7E). Using GPS-SUMO, we predicted the sumoylation sites on RCOR2, identifying lysine 60 (K60), lysine 88 (K88), and lysine 223 (K223) as potential sites for sumoylation modifications. Subsequently, we substituted the lysines at positions 60, 88, and 223 with arginine (K60R, K88R, K223R). The Ni-NTA pull-down experiment revealed the absence of the sumoylation modification band of RCOR2 in the K60R group, indicating that K60 is the sumoylation modification site of RCOR2 (figure 7F), consistent with the findings of Hendriks *et al*.[25] These experimental results suggest that the K60 site of RCOR2 can be modified by SUMO2.

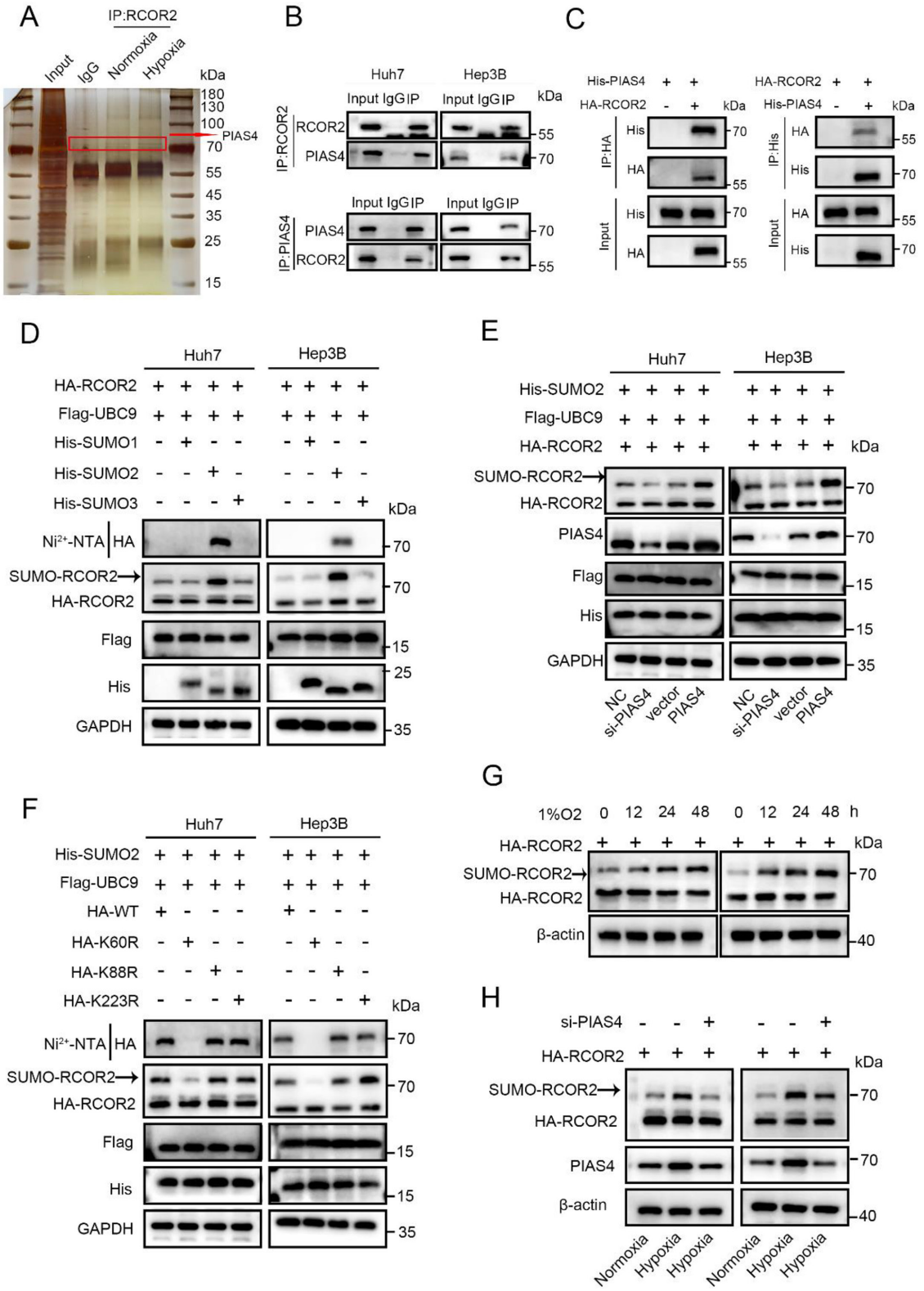

Figure 7 Hypoxia enhances the SUMOylation of RCOR2 by upregulating PIAS4. (A) Immunoprecipitation was performed in Hep3B cells and detection by silver staining. The specific bands were marked with arrows. (B) The co-immunoprecipitation experiment demonstrates that RCOR2 physically interacts with PIAS4 in hepatocellular carcinoma cells. (C) Co-immunoprecipitation assay in HEK-293T cells co-transfected with HA-tagged RCOR2 and His-tagged PIAS4 plasmids showed that RCOR2 can directly interact with PIAS4. (D) An Ni-NTA pull-down assay was conducted to identify the specific type of sumoylation of RCOR2. (E) Western blot analysis was conducted to detect the regulatory effect of PIAS4 on the sumoylation of RCOR2. (F) Ni-NTA pull-down experiments validate the sumoylation site of RCOR2. (G) The western blot results indicate that hypoxia enhances the sumoylation modification of RCOR2. (H) PIAS4 knockdown inhibits the promoting effect of hypoxia on the sumoylation of RCOR2. RCOR2, REST corepressor 2.

Subsequently, we examined the regulatory effects of hypoxic conditions on the ubiquitination of RCOR2. Western blot experiments demonstrated that the level of RCOR2 sumoylation in cells increased with prolonged exposure to hypoxia (figure 7G). Concurrently, hypoxia enhanced the expression of PIAS4 in HCC cells (online supplemental figure S10C). We also investigated whether the hypoxic environment influences the sumoylation of RCOR2 through PIAS4. The knockdown of PIAS4 reversed the regulatory effect of hypoxia on the sumoylation of RCOR2 (figure 7H). These findings suggest that the hypoxic environment promotes the sumoylation of RCOR2 by upregulating the expression of PIAS4.

Hypoxia promotes the stability and nuclear translocation of the RCOR2 protein by enhancing its SUMOylation

The results of the protein stability experiments suggest that SUMOylated RCOR2 exhibits a high degree of stability (figure 8A). Meanwhile, the application of the protease inhibitor MG132 prevents the degradation of non-SUMOylated RCOR2 (figure 8B), indicating that SUMOylation may impede the proteolytic degradation of RCOR2. The detection of ubiquitination reveals that RCOR2 undergoes K48 ubiquitination modification (online supplemental figure S11A), suggesting that SUMOylation may enhance the stability of RCOR2 in a ubiquitin-dependent manner. Subsequent assessment of the ubiquitination levels of RCOR2 indicated that following transfection with SUMO2, the ubiquitination level of RCOR2-WT decreased. In the RCOR2-K60R group, both ubiquitination and sumoylation modifications were absent simultaneously. This suggests that the ubiquitination modification site of RCOR2 is also at K60, and that sumoylation inhibits the ubiquitination modification of RCOR2 by competing for the K60 site (figure 8C). Additionally, it was observed that hypoxic conditions suppressed the ubiquitination levels of RCOR2, while the knockdown of PIAS4 restored this inhibitory effect (figure 8D). Collectively, these results indicate that under hypoxic conditions, the promotion of SUMOylation modifications of RCOR2 serves to inhibit its ubiquitin-mediated degradation.

Immunofluorescence analysis demonstrated that in the SUMO2 overexpression group, RCOR2 was predominantly localized in the nucleus of HCC cells (figure 8E). Therefore, we hypothesize that the sumoylation modification of RCOR2 may facilitate its nuclear translocation. Nuclear-cytoplasmic separation experiments indicated that SUMOylated RCOR2 was primarily localized in the cell nucleus (figure 8F). Furthermore, we investigated the distribution of RCOR2 in hypoxic cells. Immunofluorescence analysis revealed that RCOR2 underwent nuclear translocation in hypoxic HCC cells compared with normoxic HCC cells. Notably, the knockdown of PIAS4 suppressed the promoting effect of hypoxia on RCOR2 nuclear translocation (figure 8G). The results from the nuclear-cytoplasmic separation experiments were consistent with the immunofluorescence findings (figure 8H). These results suggest that hypoxia enhances RCOR2 nuclear translocation in HCC cells by promoting RCOR2 sumoylation.

We further investigated the regulatory effect of SUMOylated RCOR2 on LIF expression. The results indicated that SUMO2 overexpression enhanced LIF expression (figure 8I). The knockdown of RCOR2 or PIAS4 reversed the stimulatory effect of hypoxia on LIF expression (figure 8J). This suggests that hypoxia promotes LIF expression by increasing RCOR2 SUMOylation.

Finally, we investigated whether RCOR2 regulates macrophage polarization through SUMOylation. Results from flow cytometry, qRT-PCR, and ELISA experiments demonstrated that the knockdown of PIAS4 inhibited the enhancing effect of RCOR2 overexpression on macrophage M2 polarization (online supplemental figure S12A–D). This indicates that RCOR2 SUMOylation can promote macrophage M2 polarization.

The RCOR2/LIF axis is involved in PD-1 resistance

Considering the roles of RCOR2 and LIF in regulating TAM polarization and $CD8^+$ T-cell exhaustion, we hypothesize that the RCOR2/LIF axis may play a significant role in resistance to PD-1 therapy. We employed subcutaneous tumor models and an orthotopic tumor transplantation model to investigate the regulatory function of the RCOR2/LIF axis on the efficacy of PD-1 treatment (figure 9A). The results demonstrated that RCOR2 knockdown, in combination with PD-1 treatment, significantly inhibited tumor growth. Conversely, LIF overexpression diminished the synergistic effect of RCOR2 knockdown on PD-1 treatment. Additionally, RCOR2 overexpression inhibited the therapeutic efficacy of PD-1, while LIF knockdown restored the inhibitory effect of RCOR2 overexpression on PD-1 treatment (figure 9B–D). These findings suggest that the RCOR2/LIF axis exerts a strong synergistic effect in PD-1 therapy.

DISCUSSION

The hypoxic microenvironment is a critical factor influencing immune evasion. Through RNA-seq of hypoxic cells and analysis of the TCGA database, we identified the factor RCOR2, which regulates immune evasion in the tumor hypoxic microenvironment. Clinical data analysis revealed that RCOR2 is upregulated in HCC and is associated with poor prognosis. Additionally, RCOR2 is negatively correlated with $CD8^+$ T-cell infiltration. In vivo and in vitro functional experiments demonstrated that RCOR2 promotes cell proliferation and metastasis under hypoxic conditions. Based on these findings, RCOR2 may serve as a key factor in the hypoxic environment that facilitates immune evasion in HCC, as well as a potential oncogene and biomarker for the prognosis of patients with HCC.

Tumors retain active glycolytic capabilities even in the presence of excess oxygen, demonstrating a phenomenon known as aerobic glycolysis. This process supplies energy

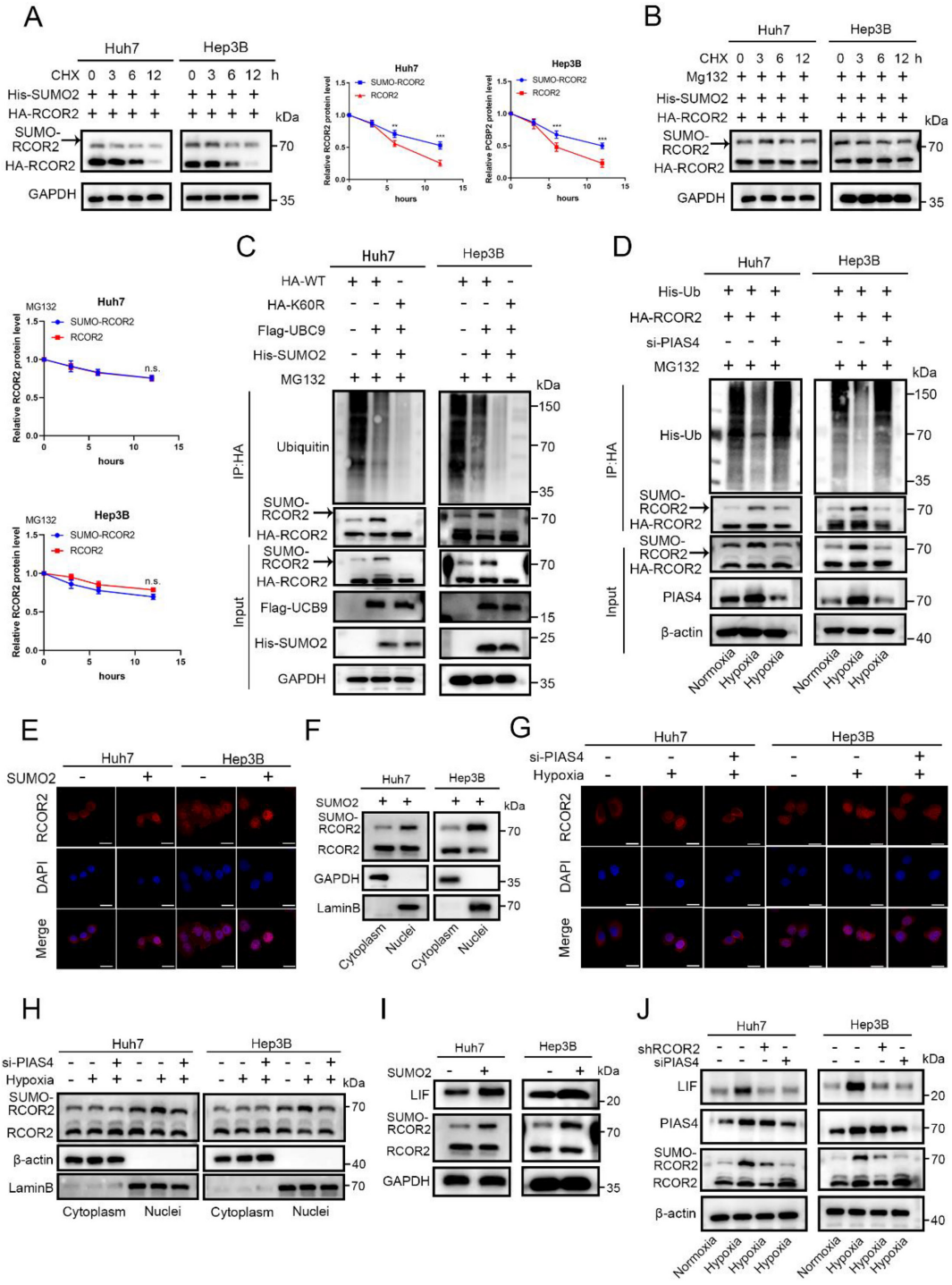

Figure 8 Hypoxia promotes the stability and nuclear translocation of the RCOR2 protein by enhancing its SUMOylation. (A) The Western blot analysis indicates that SUMOylated RCOR2 is more stable than unmodified RCOR2. (B) The western blot analysis indicates that MG132 enhances the protein stability of unmodified RCOR2. (C) Ubiquitination detection indicates that the transfection of SUMO2 can inhibit the ubiquitination modification of RCOR2 by competitively binding to the K60 site. (D) Ubiquitination detection reveals that the inhibition of PIAS4 can reverse the suppressive impact of hypoxia on the ubiquitination of RCOR2. (E) Immunofluorescence analysis demonstrates that transfection of SUMO2 enhances the nuclear translocation of RCOR2. Scale bar: 50 µm. (F) The nuclear-cytoplasmic separation experiment detects the distribution of RCOR2 between the nucleus and cytoplasm. (G) Immunofluorescence analysis reveals that hypoxia enhances the nuclear translocation of RCOR2. Knocking down PIAS4 can counteract the hypoxia-induced promotion of RCOR2 nuclear translocation. Scale bar: 50 µm. (H) The nuclear-cytoplasmic separation experiment detects the distribution of RCOR2 in hypoxic hepatocellular carcinoma cells. (I) The western blot experiment demonstrated that the overexpression of SUMO2 enhanced the expression of LIF. (J) Hypoxia enhances the expression of LIF, and the knockdown of RCOR2 or PIAS4 can reverse the stimulatory effect of hypoxia on LIF expression. Bar graphs represent mean±SEM (n=3, **p<0.01, and ***p<0.001). DAPI, 4',6-diamidino-2'-phenylindole; LIF, leukemia inhibitory factor; RCOR2, REST corepressor 2.

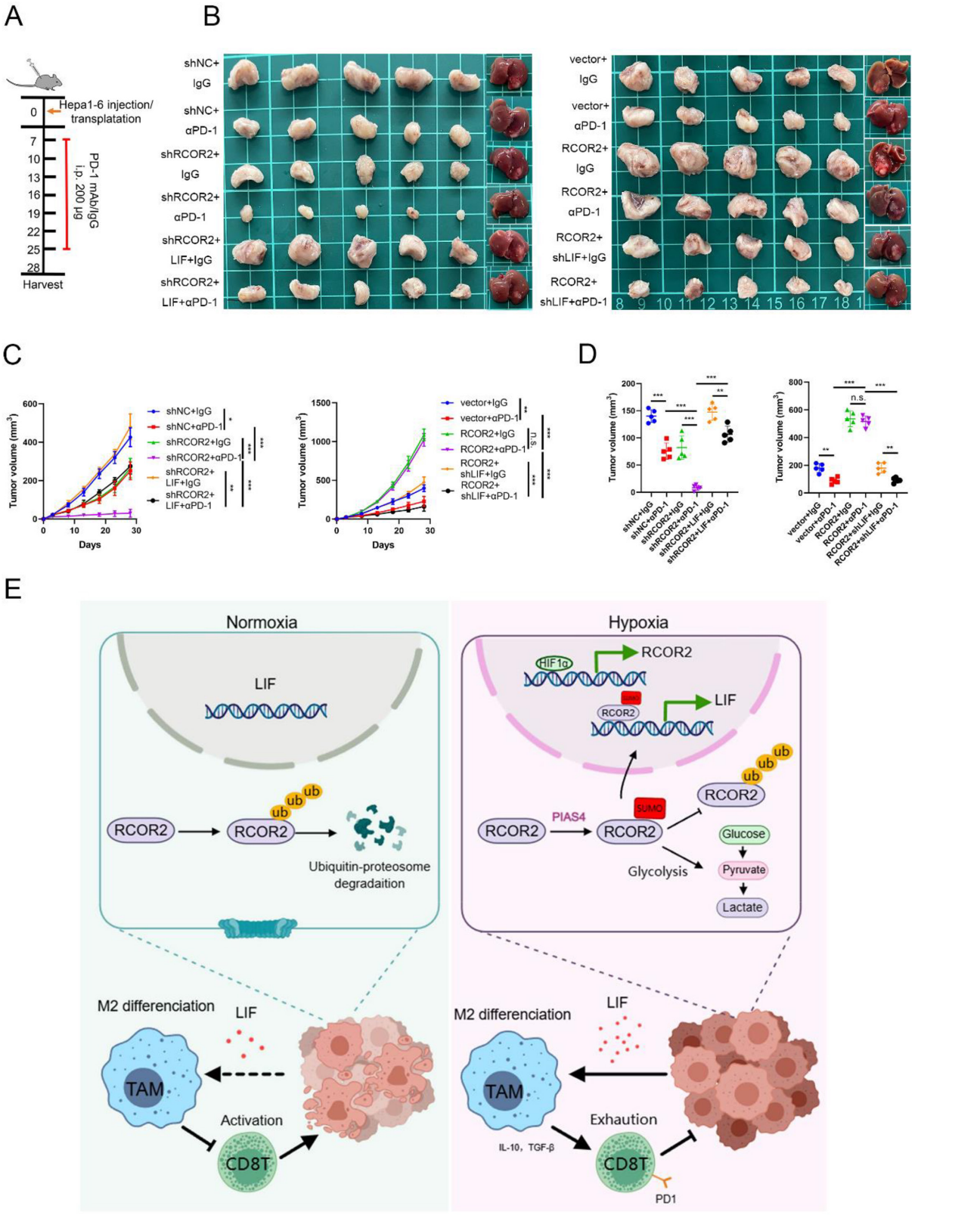

Figure 9 The RCOR2/LIF axis is involved in PD-1 resistance. (A) Schematic view of the PD-1 treatment plan in subcutaneous tumors and orthotopic tumors. (B) Representative images of subcutaneous tumors and orthotopic tumors. (C) Growth curve of subcutaneous tumors. (D) Volume of orthotopic tumors. (D) The schematic diagram illustrates the mechanism of action of RCOR2 in hepatocellular carcinoma. Bar graphs represent mean±SEM (*p<0.05, **p<0.01, and ***p<0.001). IL, interleukin; LIF, leukemia inhibitory factor; PD-1, programmed cell death protein 1; RCOR2, REST corepressor 2; TAM, tumor-associated macrophage; TGF, transforming growth factor.

for tumor cell growth, facilitating continuous proliferation, a concept referred to as the "Warburg effect".[26] Metabolic intermediates produced during aerobic glycolysis can be used for the biosynthesis of tumor biomacromolecules, thereby satisfying the demands of rapid tumor growth. The accumulation of lactic acid contributes to an acidic microenvironment that promotes cancer invasion and metastasis.[27 28] Through RNA-seq analysis, we discovered that RCOR2 plays a crucial role in regulating glycolysis in HCC cells. RCOR2 enhances ATP production, lactate generation, and glucose uptake in HCC cells under hypoxic conditions, while simultaneously decreasing the OCR. By promoting glycolysis, RCOR2 provides essential energy for the growth of HCC cells. However, this study primarily focused on the regulatory role of RCOR2 in glycolysis within HCC cells, and the specific regulatory mechanisms warrant further investigation.

RCOR2 has been reported to play a significant role in immune regulation. Through experiments involving primary HCC induction and orthotopic tumor transplantation model, we discovered that RCOR2 promotes the M2 polarization of HCC macrophages and facilitates the functional exhaustion of $CD8^+$ T cells. However, in vitro experiments indicated that knocking down or overexpressing RCOR2 in HCC cells does not directly regulate $CD8^+$ T-cell function; rather, it influences macrophage polarization. Macrophages can be classified into classically activated (M1) macrophages and alternatively activated (M2) macrophages. M1 macrophages produce pro-inflammatory cytokines and initiate immune responses against tumor cells, whereas M2 macrophages typically exhibit an immunosuppressive phenotype that promotes tumor progression.[29 30] Previous studies have demonstrated that M2 macrophages exert an inhibitory effect on $CD8^+$ T cells. On one hand, the physical barrier formed by TAMs restricts T-cell entry into the TME.[31] On the other hand, TAMs can inhibit $CD8^+$ T-cell function by expressing the immune checkpoint ligand PD-L1,[32] secreting immunosuppressive cytokines,[33] and limiting the metabolites necessary for T-cell proliferation.[34] Our study found that HCC cells overexpressing RCOR2 can enhance the expression of IL-10, TGF-β, and AGR1 in macrophages. RCOR2 promotes $CD8^+$ T-cell functional exhaustion by facilitating macrophage polarization.

RCOR2 was initially identified as a co-repressor of REST, playing a role in transcriptional repression. However, subsequent studies have demonstrated that RCOR2 also possesses transcriptional activity. Xia *et al* discovered that RCOR2 can directly activate Runx1, thereby participating in the regulation of leukemia-initiating cell differentiation in mice.[17] By analyzing RCOR2 ChIP-seq and RNA-seq data, we found that LIF is a downstream factor regulated by RCOR2 during macrophage polarization. RCOR2 enhances the transcription and secretion of LIF by binding to the LIF promoter. LIF is a member of the IL-6 cytokine family and is associated with the progression of various tumors. Studies have demonstrated that LIF is highly expressed in numerous solid tumors, including breast cancer, colorectal cancer, and pancreatic cancer.[35–37] Elevated circulating levels of LIF are correlated with tumor recurrence and resistance to radiation therapy.[35] Additionally, LIF plays a crucial role in tumor immune regulation, as the LIF receptor is abundantly expressed in macrophages. LIF enhances the immunosuppressive capacity of macrophages by binding to its receptor.[38] In tumors exhibiting high levels of LIF expression, inhibiting LIF can decrease the expression of CD206, CD163, and CCL2 in TAMs while inducing the expression of CXCL9. Blocking LIF alleviates the epigenetic silencing of CXCL9, which can stimulate the infiltration of CD8+T cells into the TME.[39] Our study further confirmed that LIF plays a crucial role in regulating the M2 polarization of macrophages. RCOR2 enhances the transcription and secretion of LIF in HCC cells, thereby promoting immune evasion in HCC.

Research indicates that HIF1α can promote the transcription of RCOR2.[17 23] Our study further demonstrates that hypoxic environments enhance RCOR2 expression through HIF1α. Additionally, MS analysis reveals that the hypoxic microenvironment facilitates the binding of RCOR2 to PIAS4. Previous studies have shown that PIAS4 can modify the sumoylation of the CoREST family.[24] However, there has been no research investigating the sumoylation of RCOR2 under hypoxic conditions. We found that hypoxic conditions promote RCOR2 sumoylation by increasing PIAS4 expression. Sumoylation modifications enhance protein stability by inhibiting ubiquitination and also facilitate the nuclear translocation of RCOR2. Hypoxia enhances the transcriptional activity of RCOR2 through sumoylation, thereby promoting the expression of LIF and facilitating the M2 polarization of macrophages.

PD-(L)1 mAb has demonstrated efficacy in patients with various advanced malignancies. However, only a small percentage of patients with HCC respond to PD-(L)1 mAb treatment.[40 41] Consequently, alternative strategies, such as combination therapies, have been extensively investigated. In this study, we identified the RCOR2/LIF axis as a key regulator of macrophage M2 polarization, which contributes to $CD8^+$ T-cell exhaustion. We further explored the regulatory role of the RCOR2/LIF axis in the context of PD-1 therapy. Using both subcutaneous and orthotopic tumor models, we validated the synergistic effect of RCOR2 knockdown in conjunction with PD-1 monoclonal antibody treatment, while LIF overexpression was found to inhibit this synergy. In a primary HCC induction model, we used AAV-8 as a vector to facilitate the overexpression of liver RCOR2. However, further development of therapeutic vectors targeting RCOR2 is necessary to evaluate their safety and potential as antitumor agents.

CONCLUSION

The hypoxia-related factor RCOR2 is upregulated in HCC and is associated with a poor prognosis. RCOR2 enhances

glycolysis in HCC cells, thereby promoting their proliferation and metastasis. Additionally, RCOR2 facilitates the M2 polarization of macrophages and contributes to $CD8^+$ T-cell exhaustion by enhancing LIF transcription. The hypoxic microenvironment inhibits the ubiquitin-mediated degradation of RCOR2 by promoting its sumoylation, which facilitates its translocation to the nucleus (figure 9E). The RCOR2/LIF axis is implicated in resistance to PD-1. Our study identifies new potential targets for immunotherapy in HCC.

Author affiliations
[1]Hepatobiliary Center, The First Affiliated Hospital of Nanjing Medical University, Nanjing, Jiangsu, China
[2]Key Laboratory of Liver Transplantation, Chinese Academy of Medical Sciences; National Health Commission (NHC) Key Laboratory of Hepatobiliary cancers, Nanjing, Jiangsu, China
[3]Department of Hepatobiliary Surgery, The Affiliated Wuxi No.2 People's Hospital of Nanjing Medical University, Wuxi, Jiangsu, China
[4]Department of Hepatobiliary Pancreatic Spleen Surgery, Affiliated Hospital of Jiangsu University, Zhenjiang, Jiangsu, China

Contributors WJ and JW conducted the primary tasks of the molecular laboratory experiments, contributed to data analysis, and participated in the research design. The manuscript was drafted by WJ. WY, ZD, LL, and CX were involved in the experimental work. YF, QL, and YY analyzed the experimental data. DZ, WZ, and XL collected the clinical data. XA, YZ, LK, and WD conceived and coordinated the research. WD was the guarantor of the study. All authors reviewed and approved the final manuscript.

Funding This work was supported by grants from the National Natural Science Foundation of China (81871260); The training program of "Double Hundred" young and middle-aged medical and health talents in Wuxi (BJ020034); "Light of Taihu Lake" scientific and technological research project of the Wuxi Science and Technology Bureau (Y20222002); Young Scholars Fostering Fund of the First Affiliated Hospital of Nanjing Medical University (PY2022007); Postgraduate Research & Practice Innovation Program of Jiangsu Province 40 (SJCX23_0688; SJCX24_0730; SJCX22_0645); Medical research project of Jiangsu Provincial Health Commission (M2024017). All funding sources had no involvement in any of the following aspects: study design; collection, analysis, or interpretation of data; writing of the manuscript; or decisions related to submission for publication.

Competing interests No, there are no competing interests.

Patient consent for publication Not applicable.

Ethics approval The study protocol was approved by the Institutional Review Board of the First Affiliated Hospital of Nanjing Medical University. Ethics Committee of the First Affiliated Hospital of Nanjing Medical University exempted consent for participation in the study (No.2023-SRFA-364).

Provenance and peer review Not commissioned; externally peer reviewed.

Data availability statement Data are available in a public, open access repository. Data are available upon reasonable request.

ORCID iD
Wenzhou Ding http://orcid.org/0009-0003-3734-7112

REFERENCES

1 Bray F, Laversanne M, Sung H, *et al*. Global cancer statistics 2022: GLOBOCAN estimates of incidence and mortality worldwide for 36 cancers in 185 countries. *CA Cancer J Clin* 2024;74:229–63.
2 Llovet JM, Zucman-Rossi J, Pikarsky E, *et al*. Hepatocellular carcinoma. *Nat Rev Dis Primers* 2016;2.
3 Shao C, Yang F, Miao S, *et al*. Role of hypoxia-induced exosomes in tumor biology. *Mol Cancer* 2018;17:120.
4 Chen Z, Han F, Du Y, *et al*. Hypoxic microenvironment in cancer: molecular mechanisms and therapeutic interventions. *Signal Transduct Target Ther* 2023;8:70.
5 Koukourakis MI, Giatromanolaki A, Skarlatos J, *et al*. Hypoxia inducible factor (HIF-1a and HIF-2a) expression in early esophageal cancer and response to photodynamic therapy and radiotherapy. *Cancer Res* 2001;61:1830–2.
6 Guan Y, Reddy KR, Zhu Q, *et al*. G-rich oligonucleotides inhibit HIF-1alpha and HIF-2alpha and block tumor growth. *Mol Ther* 2010;18:188–97.
7 Harris AL. Hypoxia--a key regulatory factor in tumour growth. *Nat Rev Cancer* 2002;2:38–47.
8 Barsoum IB, Smallwood CA, Siemens DR, *et al*. A mechanism of hypoxia-mediated escape from adaptive immunity in cancer cells. *Cancer Res* 2014;74:665–74.
9 Chang C-H, Qiu J, O'Sullivan D, *et al*. Metabolic Competition in the Tumor Microenvironment Is a Driver of Cancer Progression. *Cell* 2015;162:1229–41.
10 Leone RD, Powell JD. Metabolism of immune cells in cancer. *Nat Rev Cancer* 2020;20:516–31.
11 Nakaya M, Xiao Y, Zhou X, *et al*. Inflammatory T cell responses rely on amino acid transporter ASCT2 facilitation of glutamine uptake and mTORC1 kinase activation. *Immunity* 2014;40:692–705.
12 Munn DH, Shafizadeh E, Attwood JT, *et al*. Inhibition of T cell proliferation by macrophage tryptophan catabolism. *J Exp Med* 1999;189:1363–72.
13 Srivastava MK, Sinha P, Clements VK, *et al*. Myeloid-derived suppressor cells inhibit T-cell activation by depleting cystine and cysteine. *Cancer Res* 2010;70:68–77.
14 Bader JE, Voss K, Rathmell JC. Targeting Metabolism to Improve the Tumor Microenvironment for Cancer Immunotherapy. *Mol Cell* 2020;78:1019–33.
15 Wang Y, Wu Q, Yang P, *et al*. LSD1 co-repressor Rcor2 orchestrates neurogenesis in the developing mouse brain. *Nat Commun* 2016;7:10481.
16 Negrini S, Prada I, D'Alessandro R, *et al*. REST: an oncogene or a tumor suppressor? *Trends Cell Biol* 2013;23:289–95.
17 Xia F, Zhang Y, Xie L, *et al*. B7-H4 enhances the differentiation of murine leukemia-initiating cells via the PTEN/AKT/RCOR2/RUNX1 pathways. *Leukemia* 2017;31:2260–4.
18 Xiong Y, Wang L, Di Giorgio E, *et al*. Inhibiting the coregulator CoREST impairs Foxp3+ Treg function and promotes antitumor immunity. *J Clin Invest* 2020;130:131375:1830–42:.
19 Bhave VS, Paranjpe S, Bowen WC, *et al*. Genes inducing iPS phenotype play a role in hepatocyte survival and proliferation in vitro and liver regeneration in vivo. *Hepatology* 2011;54:1360–70.
20 Zhu G, Liu W, Shi Y, *et al*. Single cell rna-seq of cancer-associated fibroblasts in hbv-related hepatocellular carcinoma. 2023 Available: https://www.ncbi.nlm.nih.gov/geo/query/acc.cgi?acc=GSE202642
21 ENCODE Database. ENCODE project consortium. tf chip-seq in hepg2. 2016. Available: https://www.encodeproject.org/experiments/ENCSR455DOO
22 ENCODE project consortium. Control chip-seq in hepg2. ENCODE Database; 2016. Available: https://www.encodeproject.org/experiments/ENCSR239QGH
23 Hagan T, Gerritsen B, Tomalin LE, *et al*. Transcriptional atlas of the human immune response to 13 vaccines reveals a common predictor of vaccine-induced antibody responses. *Nat Immunol* 2022;23:1788–98.
24 Sáez JE, Arredondo C, Rivera C, *et al*. PIASγ controls stability and facilitates SUMO-2 conjugation to CoREST family of transcriptional co-repressors. *Biochem J* 2018;475:1441–54.
25 Hendriks IA, D'Souza RCJ, Yang B, *et al*. Uncovering global SUMOylation signaling networks in a site-specific manner. *Nat Struct Mol Biol* 2014;21:927–36.
26 Warburg O. On respiratory impairment in cancer cells. *Science* 1956;124:269–70.

27 Feng J, Li J, Wu L, *et al*. Emerging roles and the regulation of aerobic glycolysis in hepatocellular carcinoma. *J Exp Clin Cancer Res* 2020;39.
28 Ganapathy-Kanniappan S, Geschwind J-F. Tumor glycolysis as a target for cancer therapy: progress and prospects. *Mol Cancer* 2013;12.
29 DeNardo DG, Ruffell B. Macrophages as regulators of tumour immunity and immunotherapy. *Nat Rev Immunol* 2019;19:369–82.
30 Mantovani A, Marchesi F, Malesci A, *et al*. Tumour-associated macrophages as treatment targets in oncology. *Nat Rev Clin Oncol* 2017;14:399–416.
31 Peranzoni E, Lemoine J, Vimeux L, *et al*. Macrophages impede CD8 T cells from reaching tumor cells and limit the efficacy of anti-PD-1 treatment. *Proc Natl Acad Sci U S A* 2018;115:E4041–50.
32 Kuang D-M, Zhao Q, Peng C, *et al*. Activated monocytes in peritumoral stroma of hepatocellular carcinoma foster immune privilege and disease progression through PD-L1. *J Exp Med* 2009;206:1327–37.
33 Rodriguez PC, Quiceno DG, Zabaleta J, *et al*. Arginase I production in the tumor microenvironment by mature myeloid cells inhibits T-cell receptor expression and antigen-specific T-cell responses. *Cancer Res* 2004;64:5839–49.
34 Rodriguez PC, Zea AH, DeSalvo J, *et al*. L-arginine consumption by macrophages modulates the expression of CD3 zeta chain in T lymphocytes. *J Immunol* 2003;171:1232–9.
35 Liu S-C, Tsang N-M, Chiang W-C, *et al*. Leukemia inhibitory factor promotes nasopharyngeal carcinoma progression and radioresistance. *J Clin Invest* 2013;123:63428:5269–83:.
36 Yu H, Yue X, Zhao Y, *et al*. LIF negatively regulates tumour-suppressor p53 through Stat3/ID1/MDM2 in colorectal cancers. *Nat Commun* 2014;5.
37 Shi Y, Gao W, Lytle NK, *et al*. Targeting LIF-mediated paracrine interaction for pancreatic cancer therapy and monitoring. *Nature New Biol* 2019;569:131–5.
38 Hallett RM, Bonfill-Teixidor E, Iurlaro R, *et al*. Therapeutic Targeting of LIF Overcomes Macrophage-mediated Immunosuppression of the Local Tumor Microenvironment. *Clin Cancer Res* 2023;29:791–804.
39 Pascual-García M, Bonfill-Teixidor E, Planas-Rigol E, *et al*. LIF regulates CXCL9 in tumor-associated macrophages and prevents $CD8^+$ T cell tumor-infiltration impairing anti-PD1 therapy. *Nat Commun* 2019;10.
40 D'Alessio A, Cammarota A, Prete MG, *et al*. The evolving treatment paradigm of advanced hepatocellular carcinoma: putting all the pieces back together. *Curr Opin Oncol* 2021;33:386–94.
41 Finn RS, Ryoo B-Y, Merle P, *et al*. Pembrolizumab As Second-Line Therapy in Patients With Advanced Hepatocellular Carcinoma in KEYNOTE-240: A Randomized, Double-Blind, Phase III Trial. *J Clin Oncol* 2020;38:193–202.